CALIFORNIA STATE UNIVERSITY, NORTHRIDGE

MAGNETOSTRATIGRAPHIC AND STABLE ISOTOPIC ANALYSIS OF PLAYA-LACUSTRINE DEPOSITS IN THE QAIDAM BASIN, CHINA: IMPLICATIONS FOR CLIMATE-ENVIRONMENTAL CHANGES AND ORBITAL FORCING MECHANISMS DURING THE PLIO-QUATERNARY TRANSITION

A thesis submitted in partial fulfillment of the requirements

for the degree of Master of Science in Geology

By

Annelisa Ehret Moe

May 2017

The thesis of Annelisa Ehret Moe is approved:

_____	_____
Vicki Pedone, Ph.D.	Date
_____	_____
Jennifer Cotton, Ph.D.	Date
_____	_____
Richard Heermance, Ph.D., Chair	Date

California State University, Northridge

PREFACE

Compiling a Pliocene-Quaternary climate record is complicated because Earth has experienced substantial climate variability over the past 5 million years, including a long-term cooling trend (the Plio-Quaternary transition) as well as short-term cyclical climate fluctuations driven by orbital forcing. While benthic records of the effects of short-term variation within this transition are well documented, the effects of these variations are not well understood or well constrained for terrestrial settings. The purpose of this study is to investigate these short-term environmental impacts of the long-term climatic transition from the warm, wet, lake-dominated conditions of the Miocene epoch to the cold, dry, playa-dominated conditions observed within the Qaidam Basin today. The Qaidam Basin provides an ideal location for high-resolution sampling of high-elevation terrestrial Plio-Quaternary deposition owing to the thick sections of exposed and preserved strata which represent shifting depositional environments within the basin during the past 5 million years.

This project was completed in collaboration with Carmala Garzione and her students Lin Li and Rebecca Kreuzer from Rochester University in New York, and with Junsheng Nie and his students Lou Zeng and Qingda Su from Lanzhou University in China. Measurement and description of the stratigraphic section were completed by Richard Heermance, Lou Zeng and Lin Li. Samples were collected by Junsheng Nie, Lou Zeng and Qingda Su. Some samples were sent to Rochester University, where they were processed for stable isotope analysis by Rebecca Kreuzer.

The rest of the samples were sent to CSU Northridge, where my contributions to this project began. I processed remaining samples for paleomagnetic analysis and

correlation to the GPTS. I also combined stratigraphy notes to create a composite stratigraphic column, and analyzed this stratigraphy for environmental patterns and lake level cyclicity. Finally, I also received the stable isotope data from Rebecca Kreuzer, and analyzed the δ18O data for climatic trends and cyclicity. This paper presents the results of the magnetostratigraphic geochronology, the sedimentological record, and the δ18O stable isotopic record to discuss the Qaidam Basin evolution as well as its associated climatic trends and its response to orbital forcing mechanisms.

This submission includes a table of contents, an abstract, the main text of the paper, figures (Appendix A), tables (Appendix B), an extended discussion about orbital controls on climate cyclicity (Appendix C), a detailed discussion of what is known about lake evolution in the Qaidam Basin (Appendix D), a brief overview for magnetostratigraphic analysis of sedimentary rocks (Appendix E), and a detailed methods section (Appendix F).

ACKNOWLEDGEMENTS

This project was funded primarily by NSF project #1348075, and in part by the 2016 Hannah Summer Research Award. I would like to start my long list by thanking my advisor, Dr. Richard Heermance. He is the reason I even got involved with this amazing project. His encouragement and guidance have led me through this project and pushed me to find new perspectives and to explore every exciting conclusion. Working with Dr. Heermance, I not only learned new skills and concepts, but I was also able to travel to new places and experience new cultures while traveling through China.

I would also like to thank all of my collaborators, without whom my project would not exist. Dr. Junsheng Nie from Lanzhou University coordinated and led my second trip to China and helped me to decipher the oxygen isotope data. His students, Qingda Su and Lou Zeng collected data and samples during multiple field seasons. Dr. Carmie Garzione from Rochester University and her students Lin Li and Rebecca Kreuzer collected data in the field and performed stable isotopic analysis on the samples used in my thesis. Dr. Ulrich Salzmann from Northumbria University and his student Florian Schwarz braved the cold weather to accompany me on my final field season.

I would like to thank Scott Bogue, who runs the Paleomagnetic Lab at Occidental College, for coming to my rescue on many occasions (even on the weekends) when issues arose. I would also like to thank both Dr. Vicki Pedone and Dr. Jen Cotton for joining my thesis committee and providing amazing insight into my work.

Finally, I would like to thank my family and my friends. Most importantly I would like to thank my husband, Alex. I would not have made it through this crazy adventure without his love, support and encouragement.

DEDICATION

For Alex.

TABLE OF CONTENTS

ABSTRACT

MAGNETOSTRATIGRAPHIC AND STABLE ISOTOPIC ANALYSIS OF PLAYA-LACUSTRINE DEPOSITS IN THE QAIDAM BASIN, CHINA: IMPLICATIONS FOR CLIMATE-ENVIRONMENTAL CHANGES AND ORBITAL FORCING MECHANISMS DURING THE PLIO-QUATERNARY TRANSITION

By

Annelisa Ehret Moe

Master of Science in Geology

Recently deformed and exposed strata in the Qaidam Basin provide an ideal opportunity to study environmental changes and climate variations over the past few million years. This study presents new sedimentological descriptions, magnetostratigraphy, and $\delta^{18}O$ data to investigate the timing of lake level fluctuations in the western Qaidam Basin since the middle Pliocene. Within the QC section, the study area for this project, approximately 740 m of mudstone, limestone, gypsum and halite provide a complete record of playa-lacustrine deposition. The lower 477 m were sampled for magnetostratigraphic and isotopic analysis. Magnetostratigraphy defines 9 magnetozones that correlate between 3.6 Ma and 1.8 Ma. Sedimentary and $\delta^{18}O$ data combined with our age model provides a history of environmental changes within the

basin. Prior to 3.33 Ma, QC deposition occurred in a gypsum and halite rich playa-lacustrine setting. Between 3.33 Ma and 3.1 Ma, the QC section shows lacustrine deposition, corresponding to the Mid-Piacenzian warm period. Between 3.1 Ma and 3.0 Ma, the QC section represents a gypsum rich shallow playa-lacustrine environment. After 3.0 Ma, gypsum rich playa-lacustrine deposition persists until ~1.7 Ma, when shallow playa deposition is observed. A similar trend in the QH section to the north (a previous study area) indicates basin wide responses to global climatic events such as the Mid Piacenzian warm period and the Plio-Quaternary transition towards aridification. Limestone deposition within the QC section, which is concurrent with the deposition of calcareous sandstones in the QH section, also indicates a regional shift in the hydrogeologic setting, potentially involving tectonic deformation. 65 lake cycles and 88 $\delta^{18}O$ cycles indicate that the Plio-Quaternary climate record for the Qaidam Basin may have been influenced more by eccentricity modulated precession than by obliquity, contrary to benthic $\delta^{18}O$ records. Our results suggest consistency between the stratigraphic and $\delta^{18}O$ records and show that the local effects of global climate change are site specific, depending on the sensitivity of a location to environmental perturbations. This sensitivity is likely dependent on spatial variants (i.e. elevation, topography, etc.). The results also suggest early onset aridification in the Qaidam Basin, prior to the Plio-Quaternary boundary.

1 INTRODUCTION

It is socially, economically and scientifically critical to understand Earth's climate history in order to approach the environmental uncertainties associated with the currently warming climate. Earth has experienced substantial climate variability over the past 5 million years, including a long-term cooling trend beginning ~ 5 Ma from the Miocene greenhouse conditions to the current icehouse conditions, a mid-Piacenzian (~3.3 – 3.0 Ma) warm period within this cooling trend, and short-term cyclical climate fluctuations driven by orbital forcing (McClung et al., 2013; Salzmann et al., 2011; Zachos et al., 2001). Although extensive global benthic $\delta^{18}O$ records indicate that these short-term climate fluctuations were dominated by ~41 kyr obliquity cycles prior to 1.2 Ma, recent studies in the Tibetan Plateau suggest that ~100 kyr eccentricity cycles dominated the climate record during the late Miocene and early Pliocene (Lesiecki and Raymo, 2005; Riegel et al., 2015; Saadeh et al., 2015). If these preliminary findings from high-elevation, arid, terrestrial settings are confirmed, interpretations of global climate change in terrestrial environments cannot rely exclusively on the deep marine record, but must take into account the site-specific impacts of orbital forcing.

The purpose of this study is to investigate short-term environmental impacts during the long-term climatic shift from the warmer and wetter conditions of the Pliocene epoch to the cold, dry, playa-dominated conditions observed within the Qaidam Basin today (Kezao and Bowler, 1986; Wang et al., 2012). The Qaidam Basin provides an ideal location for high-resolution sampling of high-elevation terrestrial Plio-Quaternary deposition owing to the thick sections of exposed and preserved strata which represent

shifting depositional environments within the basin during the past 5 million years (Guo et al., 2015; Heermance et al., 2013; Riegel, 2015; Zhang et al., 2012).

This work introduces a new record of environmental and climatic fluctuations in the Qaidam Basin from lithological descriptions and stable isotopic analyses. High resolution magnetic stratigraphy defines the geochronology for the strata within our study area and constrains the timing for shifts in both the lithology and the stable isotopic data. This geochronology allows for temporal correlation between data collected for this project and known global climatic events, such as wetter conditions and more negative $\delta^{18}O$ values during the Mid-Piacenzian warm period, and increasingly dry conditions coupled with high $\delta^{18}O$ values following the Plio-Quaternary boundary at ~2.6 Ma (Salzmann et al., 2011; Zachos et al., 2001). The combination of detailed sedimentology, geochronology from magnetic stratigraphy, and $\delta^{18}O$ stable isotope analysis provides a temporally continuous record of climatic and environmental cyclicity at high elevations. This reconstruction of the Pliocene-Pleistocene climate provides insight into the short-term impacts of a long-term transition between warm-wet and cold-dry conditions, evidence to suggest which factors control short-term climatic cyclicity, and implications for tectonics and the onset of aridification in the Qaidam Basin, China.

2 BACKGROUND

2.1 The Qaidam Basin

The Qaidam Basin, located in the Qinghai Provence along the northeastern margin of the Tibetan Plateau in China, is an internally drained intermontane depression that covers an area of ~120,000 km^2 with a mean elevation of 2700 m (Figure 1A). The oldest strata in the Qaidam Basin formed ~53.5 Ma, indicating that the formation of the basin initiated during the Eocene (Wang et al., 2012). Tectonic activity in this region increased through the late Cenozoic, causing dramatic uplift and forming high relief between the Qaidam Basin and the surrounding mountains (Figure 1A): the Altyn Shan to the north, the Kunlun Shan to the southwest, and the Qilian Shan to the northeast (Craddock et al., 2011; Fang et al., 2007; Wang et al., 2012). This relief provides an ideal setting for high sediment flux into the basin, forming a nearly continuous stratigraphic record of regional environmental conditions within the basin (Chen et al., 2015).

2.1.1 Qaidam Basin Lake Evolution

During the warm and wet climatic conditions of the early – middle Miocene, the northwestern region of the Qaidam Basin contained a single massive lake, or a system of large lakes, with active shorelines near the surrounding mountains along the boundaries of the basin (Kezao and Bowler, 1986; Wang et al., 2012). The shift from greenhouse to icehouse conditions in the late Miocene to early Pliocene resulted in a trend towards more arid conditions which caused this large lake to slowly dwindle and shift southeast (Kezao and Bowler, 1986; Wang et al., 2012; Zachos et al., 2001). By the late Pliocene, the northern Qaidam Basin was host to multiple small playa lakes (Heermance et al., 2013;

Kezao and Bowler, 1986). The presence and repetition of interlayered strata consisting of calcareous mudstones and evaporite formation show frequent fluctuations in lake levels within these playa lakes and alternating short-term intervals of wet and dry conditions superposed on the long-term trend towards aridification (Heermance et al., 2013; Li et al., 2013; Riegel, 2015; Wang et al., 2012).

The mountains surrounding the Qaidam Basin form a rain shadow that accentuated the trend towards aridification, leading to the hyper-arid environment observed today (Sun et al., 2008; Wang et al., 2012). Most playa lake settings within the northern Qaidam Basin completely dried up in the Holocene (Kezao and Bowler, 1986, Wang et al., 2012). Current playa lake settings within the Qaidam Basin, shown in Figure 1A, are highly saline and largely constrained to the karst zone in the southern region of the Qaidam Basin, north of Golmud (Lowenstein and Risacher, 2009; Zhang et al., 2015). The overall trend from a Miocene lake-dominated environment to the current playa-dominated environment is consistent with the shift from warm-wet to cold-dry conditions observed in the global benthic records during this time, but the effects of short-term (10^4 – 10^5 years) variation are not yet well understood or well constrained for terrestrial settings (Kezao and Bowler, 1986; Lesiecki and Raymo, 2005; Wang et al., 2012).

2.1.2 Field Area: The QC Section of the Qaidam Basin

Late Cenozoic stratigraphic deposition can be observed along the anticlinal flank of the QC section located at 37.7° N, 92.4° E in the northwestern margin of the Qaidam Basin (Figure 1A). Within the QC section, playa-lacustrine strata have been exposed by wind erosion and tectonic activity, and preserved by the hyper-arid environmental

conditions (Heermance et al., 2013; Rohrmann et al., 2013). The entire stratigraphic thickness exposed in the QC section, from the core of the anticline to the layer of active deposition, spans ~740 m. The QC section is a composite stratigraphic section, with a lower and an upper segment that overlap between 201 m and 226 m (Figure 1C).

2.2 The Plio-Quaternary Climate Record

2.2.1 Orbital Controls on Climate Cyclicity

While there are many factors that influence climate such as the concentration of greenhouse gases, albedo and solar radiation, the frequency of climatic fluctuation is often controlled by orbital forcing mechanisms (Zachos et al., 2001). Three mechanisms, known collectively as Milankovitch Cycles, are eccentricity: 100 kyr and 400 kyr cycles, obliquity: 41 kyr cycles, and precession: 23 kyr cycles (Ruddiman, 2008; Zachos et al., 2001). Each of these mechanisms controls the amount or distribution of solar radiation each hemisphere receives throughout the year. The dominant mechanism drives the frequency at which climate fluctuates on Earth (Berger et al., 2006; Ruddiman, 2008). Appendix D provides more details about orbital controls on climate cyclicity.

2.2.2 The Global Benthic $\delta^{18}O$ Climate Record

There are two measurable stable isotopes of the oxygen atom, ^{16}O and ^{18}O (Riebeek, 2005; Rosman 1999). ^{16}O is a lighter isotope than ^{18}O, and ^{16}O forms weaker bonds than ^{18}O (Kendall and Caldwell, 1998). Earth is an efficient system, so $H_2{}^{16}O$ is preferentially evaporated, taking lighter oxygen out of the reservoir and subsequently leaving higher percentages of heavier oxygen behind (Riebeek, 2005). These shifts in abundance can be measured and applied to the following equation:

$$\delta^{18}O = \left(\frac{\left(\frac{^{18}O}{^{16}O}\right)_{sample}}{\left(\frac{^{18}O}{^{16}O}\right)_{standard}} - 1 \right) * 1000\ ^{o}/_{oo}$$

The $\delta^{18}O$ of a reservoir is recorded in the sediment formed within that reservoir (Kendall and Caldwell, 1998). High $\delta^{18}O$ values indicate an arid climate because a higher percentage of ^{16}O is taken out of the reservoir through evaporation, increasing the relative amount of ^{18}O left behind. Lower $\delta^{18}O$ values indicate a wet climate because ^{16}O is released back into the system, lowering the relative amount of ^{18}O in the reservoir (Ruddiman, 2008).

The study of $\delta^{18}O$ in marine sediments provide an extensive record of global climatic trends and fluctuations (Zachos et al., 2001). The benthic $\delta^{18}O$ record for the past 4 million years (Figure 2A) defines the general trend of the Plio-Quaternary transition towards more cold and arid climatic conditions, and it recognizes individual short-term climate cycles throughout this time (Zachos et al., 2001). The benthic record shows ~100 kyr eccentricity dominant cycles during the past 1.2 million years (Figure 2B). Prior to this time, climatic fluctuations were dominated by ~41 kyr obliquity cycles (Figure 2A; Lesiecki and Raymo, 2005). 23 kyr precession cycles can also be seen throughout the past 4 million years, but the strength of this precession signal is weak compared to the obliquity signal in this benthic data (Lesiecki and Raymo, 2007). Therefore, obliquity is the driving force that controls the climate cycle frequency in the benthic record prior to 2.1 Ma (Zachos et al., 2001; Lesiecki and Raymo, 2007). This global benthic $\delta^{18}O$ record is extensive; however, in order to attain a thorough understanding of the global climate record, these marine records must be combined with terrestrial data.

2.2.3 The Preliminary Terrestrial $\delta^{18}O$ Climate Record

Preliminary stable isotopic analyses have been conducted in the Tibetan Plateau and the northwestern margin of the Qaidam Basin. These studies suggest 100 kyr climate cycle frequency as early as 4 Ma (Riegel et al., 2015; Saadeh et al., 2015). Figure 2C shows a frequency analysis of Qaidam Basin $\delta^{18}O$ data that identify 125 kyr cycles, with possible secondary 19 kyr and 41 kyr signals (Riegel et al., 2015). Within the Qaidam Basin, there is also evidence for the onset of aridification as early as 3.9 Ma, prior to the Plio-Quaternary Boundary (Riegel, 2015). This indicates that a high-elevation, high-relief terrestrial setting may be particularly susceptible to the effects of global aridification, owing to sensitivity to different orbital forcing mechanisms (Berger et al., 2006; Riegel, 2015; Ruddiman, 2008; Saadeh et al., 2015).

3 METHODS

3.1 Field Work

Field work in the QC section of the Qaidam Basin was conducted during three field seasons between May 2015 and December 2016. A 540-m-thick section was measured and described near the core of the anticline (Figure 1C). An additional ~200 m above this measured section were estimated and inferred to be similar material to that observed at the top of the measured section. Detailed descriptions of these ~200 m could not be made due to the presence of a thick gypsum crust. The layer of active deposition was identified at ~740 m. Between 0 and 477 m, 330 samples were collected for paleomagnetic and stable isotopic analyses, with an average sample spacing of ~2.5 m.

3.2 Magnetic Stratigraphy and Temporal Correlation

290 of the 330 collected samples were cut and processed for paleomagnetic signatures. These samples were initially processed with alternating steps of Natural Remnant Magnetization (NRM) and low temperature liquid nitrogen demagnetization (Borradaile et al., 2004; Opdyke and Channell, 1996). Then the samples were processed for Alternating Field (AF) demagnetization at 25 - 200 oersteds (oe), and for Thermal (TT) demagnetization at 150° - 530° C (Opdyke and Channell, 1996). All samples began to show high processing errors due to low magnetization by ~500° C, and were sufficiently demagnetized by ~530° C. The paleomagnetic data were analyzed using the methods of Kirschvink (1980) to identify each sample as either normal (north and down) or reverse (south and up), and to categorize each sample as either robust, tentative, or uninterpretable. Detailed methods for paleomagnetic analysis are in Appendix F.

Expected values for the samples collected in the in the QC section were determined to be declination = 0° and inclination = 56.9° for normal polarity, and declination = 180° and inclination = -56.9° for reverse polarity; see Appendix E for calculations (Opdyke and Channell, 1996). Samples with robust signatures showed two magnetic components (primary and viscous), and they generally had stratigraphic declination and inclination values that were within 10° of expected values with a Mean Angle of Deviation (MAD) value $\leq$ 10. Samples with tentative signatures showed two magnetic components, and they generally had stratigraphic declination and inclination values that were within 20° of expected values with an MAD value $\leq$ 20. Samples that did not meet these criteria were considered uninterpretable. The inclination and declination for samples with interpretable signatures were used to produce the QC magnetic stratigraphy, which was correlated to the geomagnetic polarity time scale (GPTS) to identify absolute ages for the stratigraphic height of each identified magnetic reversal event, and to determine an age range for the entire QC section (Gradstein et al., 2004).

3.3 The Stratigraphic Record

Four major depositional environments were recognized within the QC section. A playa lake depositional environment contains very shallow subaqueous deposition in an environment where evaporation is much greater than inflow, represented in the sedimentological record by mudstone with a high concentration of evaporitic material (Aref et al., 1997; Li et al., 2013). A shallow lake contains shallow subaqueous deposition in an environment where evaporation is slightly greater than inflow, represented by mudstone with a low concentration of evaporitic material (Pietras and

Carroll, 2006). A deep lake contains deep subaqueous deposition in an environment where inflow is greater than evaporation, represented by mudstone deposition (Ma et al., 2016). Finally, nearshore or shoreline deposition contains shallow subaqueous and fluvial deposition, represented by mudstone with a low concentration of evaporitic material, occasional fine sandstone with internal structures, as well as limestone that occasionally forms as stromatolites or oolites (James and Dalrymple, 2010; Miall, 2013).

Five distinct stratigraphic units were identified within the composite stratigraphic QC section, representing shifts in the depositional environment of the Qaidam Basin (Pietras and Carroll, 2006). Lake level fluctuations were interpreted within the stratigraphic record when a mudstone layer transitions to an evaporite rich mudstone layer (<50% evaporitic material) and then back into a mudstone layer, indicating shifts between deep (mudstone) and shallow (evaporite rich mudstone) lake levels (Ma et al., 2016; Pietras and Carroll, 2006). Lake level fluctuations were also identified when any mudstone dominant layer is capped by an evaporite layer that contains more that 50% evaporitic material (Aref et al., 1997; Li et al., 2013). Application of the magnetostratigraphic geochronology to the stratigraphic column can be used to calculate average sedimentation rate between each reversal event as well as the timing of lake level cyclicity and the age for significant environmental changes.

3.4 The Stable Isotopic Record

221 of the 330 collected samples were processed for oxygen isotopic analysis relative to Vienna Standard Mean Ocean Water (VSMOW), which has a value of 0 $^{0}/_{00}$ (Brand et al., 2009). Values greater than 0 $^{0}/_{00}$ (high $\delta^{18}O$ values) represent high levels of

evaporation, which indicates relatively arid conditions (Kendall and Caldwell, 1998; Ruddiman, 2008). Values less than 0 $^{0}/_{00}$ (low $\delta^{18}O$ values) represent an inflow of ^{16}O-rich water and low levels of evaporation, which indicates relatively wet conditions (Kendall and Caldwell, 1998; Ruddiman, 2008). High amplitude fluctuation between the lowest and highest $\delta^{18}O$ value indicate more dramatic environmental shifts, whereas low amplitude fluctuations indicate more stable conditions (Zachos et al., 2001). Based on these assumptions, shifts in the $\delta^{18}O$ record can be interpreted as change in regional climate during the time of sediment deposition within the Qaidam Basin (Kendall and Caldwell, 1998). The $\delta^{18}O$ data were correlated to the magnetostratigraphic geochronology, then analyzed both visually and statistically for overall climatic trends and for climate cycle frequency.

4 RESULTS

4.1 Sedimentology of the QC Section

The composite stratigraphic column for the QC section is dominated by mudstones and gypsum-rich mudstones, with interbedded evaporite and limestone layers, as well as occasional sandstone beds and lenses (Table 1; Figure 3).

4.1.1 Mudstones

M1 is a massive yellowish grey (5Y 7/2) calcareous siltstone which weathers to a brownish pink color (Figure 4A). M1 beds are laterally continuous with a common bedding thickness of 2 - 5 m, though they vary between 1 m and 15 m. The massive bedding in M1 layers indicates bioturbation likely by ostracods (Platt, 1992). M2 is a mottled light brownish grey (5YR 6/1) calcareous siltstone with interbedded 1 mm oxidized layers that range from red to orange-brown in color (Figure 4B). M2 beds are commonly 2 – 4 m thick and laterally continuous with horizontal lamination. Both of these mudstones are made up of very well sorted silt size grains, likely transported by aeolian processes, and they represent subaqueous deposition in a deep, low-energy, oxidizing, offshore lacustrine environment (James and Dalrymple, 2010; Ma et al., 2016; Wang et al., 2012). Thick mudstone layers indicate prolonged wet conditions, whereas thin layers likely represent short-term wet conditions within a generally dry period (Ma et al., 2016; Moy et al., 2002; Zachos et al., 2001).

4.1.2 Gypsum Rich Mudstones

M1/Y consists of massive siltstone (see M1 description above) containing in-situ grey chipped gypsum crystals that are 1 – 3 cm in diameter and spaced 3 – 10 cm apart

(Figure 5A). Overall, these strata contain less than 50% gypsum with increasing gypsum concentration up-section within the layer. The base of M1/Y beds are gradational with M1 beds, whereas the tops have sharp contacts with overlying beds of gypsum, halite or M1. M2/Y has similar characteristics as M1/Y, but it contains M2 rather than M1 siltstone (Figure 5B). Gypsum rich mudstones represent subaqueous deposition in a shallow lacustrine environment (Aref et al., 1997; Pietras and Carroll, 2006). The presence of an M1/Y or M2/Y layer indicates a gradual drop in lake levels followed by a rapid rise in lake levels (Li et al., 2013; Ma et al., 2016; Wang et al., 2012). Larger gypsum clasts within these layers indicate highly saline brine, and longer crystal formation time due to prolonged shallow lacustrine deposition (Aref et al., 1997; Magee et al., 1995; Schreiber and Tabakh, 2000).

M3 is a highly calcareous mottled yellow (10Y 8/3) siltstone that contains only minor (5% - 10 %) amounts of microcrystalline gypsum (Figure 5C). M3 beds are 1 – 2 m thick, and are interbedded with M1 and M2 beds, which indicates brief periods of shallow lacustrine deposition with relatively low salinity during a generally wet period with deeper lake levels (Li et al., 2013; Ma et al., 2016; Schreiber and Tabakh, 2000).

4.1.3 Evaporites: Gypsum and Halite

Y1 is a greyish orange (10YR 7/4) siltstone containing more than 50% milky white to translucent gypsum crystals (Figure 6A). Y1 beds are commonly between 10 cm and 20 cm thick. These strata are interpreted as subaqueous deposition in a shallow playa lake with relatively high salinity (Aref et al., 1997; Li et al., 2013; Pietras and Carroll, 2006; Schreiber and Tabakh, 2000). Y2 is a microcrystalline gypsum layer with thin bedding (Figure 6B), interpreted as subaqueous deposition in a playa lake with relatively

low salinity, and potentially associated with organic matter (Cody and Cody, 1988; Cooper, 1998; Schreiber and Tabakh, 2000). Y3 is a thin (5cm – 10 cm) yellowish grey (5Y 7/2) hardpan gypsum layer, interpreted as subaqueous deposition in a shallow playa lake with high salinity (Aref et al., 1997; Jutras et al., 2007; Warren, 2010).

Z1 is a massive bluish grey (5BG 5/1) halite with irregular lower and upper bedding contacts (Figure 6C). Bedding thickness for Z1 layers is thin (20 – 40 cm) except at 119 m, where thickness is 1 m. The formation of multiple halite beds interbedded with mudstone and gypsum rich mudstone indicates recurring events of flooding and evaporation to form highly concentrated brine, with Z1 representing halite formed in highly saline playa lake depocenters during low lake levels (Jutras et al., 2007; Pietras and Carroll, 2006; Schreiber and Tabakh, 2000; Warren, 2010).

4.1.4 Limestones

L1 is a thin (1 – 10 cm) medium – dark grey (N1) limestone (Figure 7). L1 layers often present as highly calcareous and resistant siltstone layers, occasionally forming hogback ridges. L1 also appears as a thin (~1 mm) laminations interbedded within thicker (10 – 30 cm) M1 layers, referred to here as M1/L1. These L1 and M1/L1 layers are interpreted as sub-aqueous deposition in a shallow lacustrine setting (de Wet et al., 2015; Stauffer and Wittchen, 1991). Occasionally L1 layers present as tufa, indicating initiation of a local spring; or as stromatolite and oolite, indicating shoreline deposition. The onset of limestone formation can be triggered by changes in many variables including water chemistry, water temperature or input of clastic sediment, all of which indicate a shifting hydrogeologic setting (de Wet et al., 2015; Pedley, 1990; Stauffer and Wittchen, 1991).

4.1.5 Sandstones

S1 is a fine-grained sandstone with trough-cross bedding (Figure 8A). The thicknesses of S1 layers vary between 10 cm and 20 cm. S2 is a thin (~ 3 cm) layer of pale orange fine sandstone with hummocky bedding contacts (Figure 8B). S3 is a thin (2 – 5 cm) discontinuous lens of fine-grained calcareous sandstone (Figure 8C). These fine-grained sandstone layers and lenses were formed in shallow channels of low gradient ephemeral streams that flowed into the shallow playa lake, which was located ~50 km from the surrounding mountains and their adjacent coarse-grained alluvial fans (Miall, 2013; Pietras and Carroll, 2006). The infrequency of these strata indicates that surface flow across the basin to the playa lake was uncommon (Wang et al., 2012). There is also a single dropstone made of fine - medium grained sandstone observed at 53.5 m in stratigraphic height (Figure 8D), indicating the presence of ice-rafting debris from a rare period when the lake was frozen (Bennett et al., 1996).

4.1.6 Stratigraphic Units

The composite stratigraphic column for the QC section shows lithofacies groupings and patterns that can be broken down into five distinct units (Figure 3; Table 2). In general, mudstones decrease up-section; and evaporites, limestones and sandstones increase up-section.

- Unit 1 (0m – 120 m) is dominated by M1 and M2, with frequent interlayered M1/Y, Y1 and Z1 beds, with a single S1 bed. The top of Unit 1 is identified by a 1-m-thick Z1 bed.

- Unit 2 (120 m – 185 m) begins with a sharp transition from Z1 to M1, and consists of thick M1 and M2 beds with two ~5-m-thick intervals of M1/Y. The top of Unit 2 is identified by the appearance and persistence of thick M1/Y and M2/Y strata.
- Unit 3 (185 m – 300 m) starts with 32 m of M1/Y and M2/Y with interbedded Y1, Y2 and Y3 beds (Unit 3A) followed by 83 m of M1 and M2 with interlayered Y1, Y2 and M1/Y beds (Unit 3B). The first appearance of L1 occurs at 267 m. The top of Unit 3 is identified by an abrupt increase in L1 strata.
- Unit 4 (300 m – 500 m) is dominated by M1 and M2, but contains frequently interbedded L1 as well as layers of Y1, Y2, M3, M1/Y and M1/L1, as well as S1, S2 and S3 increasing in frequency upsection. The top of Unit 4 is identified by the onset of thick M2/Y strata.
- Unit 5 (500 m – 540 m) contains M2/Y with interbedded L1, Y1, Y2, S1, S2 and S3.
- The remaining ~200 m of the section (540 m - ~740 m) are covered in a thick gypsum crust. However, this gypsum crust indicates significant gypsum content in the underlying strata, and therefore these ~200 m are inferred to be similar to the material observed in Unit 5. The top of the stratigraphic section (~740 m) is interpreted as the layer of active deposition.

4.2 Magnetic Stratigraphy and GPTS Correlation

235 of the 330 collected samples were processed for paleomagnetic signatures; of these, 182 provided interpretable signals (Table 3). Examples of the analysis of these samples are shown in Figure 9 for a robust normal sample (15QC61; Figure 9A), a robust reverse sample (15QC139; Figure 9B) and a tentative reverse sample (15QC127; Figure 9C). Collectively, the data pass a C quality reversal test (Figure 9D), which indicates that

the normal samples deviate from the reverse samples by 180° +/- 20° (McFadden and McElhinney, 1990). Data passing the reversal test implies that the samples sufficiently reflect primary remnant magnetization, rather than viscous components (Opdyke and Channell, 1996). The sampled QC section (0 m – 477 m) contains 9 distinct magnetozones, correlating to the GPTS between 3.6 Ma and 1.8 Ma (Figure 10). This correlation is based on two main assumptions: (1) that the observed strata are young because they are found in close proximity (~200 m) to the layer of active deposition, and (2) that the noticeable shift in lithology at ~300 m is associated with the Plio-Quaternary boundary. In addition, this correlation is preferred based on statistical analysis of the Qupydon program and based on previous paleomagnetic work in similar sections within the Qaidam Basin (Heermance et al, 2013; Lallier et al., 2013; Riegel, 2015).

The sedimentation rates were calculated for each individual magnetozone by dividing the stratigraphic thickness of each magnetozone by its time interval. These sedimentation rates range from 0.07 mm/yr to 0.57 mm/yr (Figure 11B). All of these values are reasonable sedimentation rates for the Qaidam Basin (Fang et al, 2007; Heermance et al., 2013; Zhang et al. 2012). In general, sedimentation rates between 0 and 225 m (0.2 – 0.6 mm/yr) are slightly higher than those between 225 and 475 m (0.1 to 0.4 mm/yr). Projection of the final trend in sedimentation rate (~0.2 mm/yr) also indicates that the top of the QC stratigraphic section approaches 0 Ma, consistent with the field observation that the layer of active deposition is at ~740 m in stratigraphic height. Estimated ages for each stratigraphic meter were extrapolated assuming constant sedimentation rates through each magnetozone.

4.3 Lake Cycles

The presence and repetition of distinctive facies indicate where, stratigraphically, lake level fluctuations occurred (Kezao and Bowler, 1986). Lake level fluctuations were interpreted within the stratigraphic record when a mudstone dominant layer (M1, M2, M1/Y or M2/Y) transitioned to an evaporite rich layer (M1/Y, M2/Y, M3, Y1, Y2, Y3, or Z1) and then back into a mudstone dominant layer. Each lake cycle begins at the bottom of the mudstone dominant layer, and ends at the top of evaporite rich layer. By applying the magnetostratigraphic geochronology to the stratigraphic height of each lake cycle, lake cycle periods and lake cycle frequencies were calculated. A fourier analysis of these data plotted against the calculated cycle frequencies provided a frequency analysis of the lake cycle data (Figure 12B). Mudstone layers (deep lake deposition) represent high lake levels; gypsum rich mudstone as well as limestone layers (shallow lake deposition) represent intermediate lake levels; and evaporite layers (shallow playa lake deposition) indicate low lake levels (Figure 13A).

A total of 65 lake cycles are identified within the measured QC section (Figure 13A). Within Unit 1, lake-desiccation cycle times range from 2 kyrs to 54 kyrs, with an average of 22 with a standard deviation (+/-) of 18 kyrs (Figure 11C). In Unit 2, lake levels fluctuate on a timescale of 82 +/- 21 kyrs, with values ranging from 60 kyrs to 102 kyrs. In Unit 3A, lake-desiccation cycles occur every 6 +/- 4 kyrs, ranging from 3.5 kyrs to 14.1 kyrs. Lake cycle duration increases in Unit 3B, ranging from 14 kyrs – 77 kyrs, with an average of 45 +/- 22 kyrs. Cyclicity in Unit 4 is highly variable, ranging from 4 kyrs – 177 kyrs, with an average of 38 +/- 45 kyrs. The high uncertainty in the data is due to the two occurrences of long standing high lake levels at 354.5 m (177 kyr lake cycle)

and 438 m (170 kyr lake cycle). Unit 5 cyclicity ranges from 4.4 kyr to 48.3 kyrs, with an average of 25 +/- 17. Overall, lake level cycle times range from 2 kyr to 177 kyr. There is a high frequency of short (<15 kyr) cycles (Figure 12B). ~100 kyr and ~400 kyr cycles also show relatively strong signals. ~15 kyr, ~19 kyr and ~41 kyr cycles are also recognized within this lake cycle record.

4.4 Stable Isotopes: $\delta^{18}O$

$\delta^{18}O$ cycles were determined by choosing every other sample, so that one cycle was represented by one high point to the next high point in the $\delta^{18}O$ data. A total of 88 climatic cycles are recognized in the $\delta^{18}O$ record (Figure 13B), with data ranging from -11.63‰ to +6.7‰ (Table 4). In Unit 1, $\delta^{18}O$ values fluctuate between -5.43‰ and +5.39‰. Two high value (~5‰) peaks occur at 28 m (3.54 Ma) and 86 m (3.41 Ma), approximately 130 kyrs apart. In Unit 2, $\delta^{18}O$ values become more stable. Fluctuation still occurs, but the amplitude of this fluctuation is lower and the $\delta^{18}O$ values (-5.59‰ and +2.1‰) are, on average, more negative. In Unit 3, $\delta^{18}O$ fluctuations return to higher amplitudes, ranging from -6.47‰ to +6.08‰. The highest values during this period occur at 186 m (3.10 Ma) and 197 m (3.08 Ma), approximately 20 kyrs apart. In Unit 4, the amplitude of $\delta^{18}O$ fluctuation increases dramatically between -11.63‰ and +6.66‰. On average, the $\delta^{18}O$ values seem to become slightly more positive up-section, although this apparent trend may be a product of low sampling resolution in the upper segment of the QC section.

23 more cycles are recognized in the $\delta^{18}O$ record that in the lake level fluctuation record because, during wet periods, climatic fluctuations can be recorded in the $\delta^{18}O$ of the sediment, even if lake levels do not drop far enough for significant evaporite

formation (Ruddiman, 2008; Zachos et al., 2001). Therefore, Unit 2 shows more cycles based on $\delta^{18}O$ values than based on the lithology (Figure 13). However, the resolution of the $\delta^{18}O$ data is dependent on the sampling resolution, and therefore not all of the $\delta^{18}O$ data is useful for frequency analysis. In order to identify ~20 kyr precession cycles, there has to be a minimum of two samples within a 20 kyr period. Samples for $\delta^{18}O$ analysis were taken as often as possible, but the sampling resolution was limited by availability and quality of the outcrops. By first applying the 3.6 Ma – 1.8 Ma age range to the data, temporal $\delta^{18}O$ resolution can be identified. There is high resolution (1 sample / ~10 kyrs) from 3.6 Ma – 3.4 Ma, 3.2 Ma – 2.95 Ma and 2.7 Ma – 2.5 Ma. There is low resolution sampling (~1 sample / 15 kyrs) from 3.4 Ma – 3.2 Ma, 2.5 Ma – 2.4 Ma and 2.2 Ma – 1.8 Ma. Unfortunately, no outcrops were available for sampling from 2.95 Ma – 2.7 Ma or 2.4 Ma – 2.2 Ma.

There is a tradeoff between statistical confidence and resolution within a data set. To find the balance between these two criteria, samples between 3.6 and 2.95 Ma were used to produce the $\delta^{18}O$ frequency analysis. Visual analysis of the $\delta^{18}O$ data shows that ~20 kyr cycles are recognized in the stable isotope record whenever sampling resolution is high enough to identify it (Figure 13B). This suggests that if overall sampling resolution was high enough, ~20 kyr cycles may be recognized throughout the stratigraphic section. Focusing in on this period from 3.6 Ma – 2.9 Ma, a frequency analysis reveals a weak ~41 kyr signal, with stronger signals for ~100 kyr, ~50 kyr, ~23 kyr and ~15 kyr cycles.

5 DISCUSSION

5.1 Interpretation of the Sedimentological and Stable Isotopic Data

The combination of sedimentology, sedimentation rates and $\delta^{18}O$ data are used to interpret the depositional environment and climatic setting for each of the stratigraphic units within the QC section (Figure 11). Overall, the presence of gypsum throughout the QC section as well as an increase in gypsum content at the top of the section indicates onset of aridification as well as a trend towards more arid conditions in the Qaidam Basin by at least 3.6 Ma. These generally arid conditions are interrupted from 3.33 to 3.1 Ma by a prolonged wet period possibly owing to the global climatic shift of the mid-Piacenzian, as well as intermittent wet conditions that may be due to brief but intense surges in precipitation (Liu et al., 2015; Moy et al., 2002; Salzmann et al., 2011).

5.1.1 Unit 1: Prior to 3.33 Ma

Unit 1 is dominated by mudstone, with interlayered gypsum rich mudstone, gypsum and halite beds and a single sandstone bed, indicating offshore subaqueous lacustrine deposition in a closed basin with fluctuating lake levels and evaporite precipitation (Ma et al., 2016; Li et al., 2013; Wang et al; 2012). Relatively high sedimentation rates (Figure 11B) in this low energy, offshore setting indicates allochthonous sediment flux, likely from aeolian processes that transported silt from the exposed lake shorelines into the highly saline subaqueous depocenter, located at the QC section (James and Dalrymple, 2010; Rohrmann et al., 2013). Low lake levels during this time likely promoted evaporite precipitation and concentrated sediment deposition within the lake at the QC section (Warren et al., 2010). A dropstone at ~53.5 m also indicates

that this lake may have been frozen periodically, allowing for the deposition of ice-rafting debris (Bennett et al., 1996).

The top of Unit 1 is marked by the deposition of a distinct 1-m-thick halite bed (Figure 11A), which likely formed in the depocenter of a highly saline subaqueous playa lake (Jutras et al., 2007; Warren, 2010). This is the last appearance of halite in the QC section. Above 120 m, gypsum is the only evaporite identified within the strata, indicating either (1) that 3.6 – 3.33 Ma is the most arid period observed in the QC section, or (2) that brine geochemistry is altered after 3.33 Ma, likely owing to a change in the relative position of the QC section within the lake (Casas and Lowenstein, 1989; Lowenstein and Risacher, 2009; Schreiber and Tabakh, 2000).

The presence of halite within the first 5 m of the QC section indicates that arid conditions existed in the western Qaidam Basin prior to 3.6 Ma, which is consistent with other work done in this area (Riegel, 2015). The sedimentological record indicates deposition in a highly saline subaqueous playa lake with high sediment flux transported by aeolian processes from the nearby exposed shoreline (Aref et al., 1997; Rohrmann et al., 2013).

5.1.2 Unit 2: 3.33 Ma – 3.1 Ma

Unit 2 begins with a sharp transition at 120 m from the thick halite bed back to mudstone, and a dramatic drop in sedimentation rate from 0.47 to 0.17 mm/yr. Both of these changes imply a significant lake level rise which would decrease salinity and expand the lake shoreline, isolating the QC section in a deeper lacustrine setting, further from the sediment source (Ma et al., 2016). Unit 2 is almost entirely dominated by thick

mudstone beds with only 2 thin layers of gypsum rich mudstone, indicating prolonged wet conditions (Ma et al., 2016). Throughout Unit 2, $\delta^{18}O$ values are more negative with lower amplitude fluctuation, indicating more stable and wet climatic conditions (Figure 13B; Kendall and Caldwell, 1998; Zachos et al., 2001). The presence of mudstones, the lack of evaporitic material, and the low and stable $\delta^{18}O$ data all indicate long standing high lake levels due to increased surface water flow into the basin, which may be attributed to higher precipitation in the surrounding mountains (Ma et al, 2016; Wang et al, 2012; Zachos et al., 2001). Sedimentation rates steadily increase upsection, just before the re-appearance of gypsum rich lithofacies, likely due to lake level shallowing. Gypsum rich strata at 3.1 Ma indicate the end of the stable wet conditions of Unit 2 (Aref et al., 1997; Li et al., 2013).

Between 3.33 and 3.1 Ma, the QC Section depositional environment is interpreted as a low-energy oxidizing lacustrine setting (Jiang et al., 2008; Ma et al., 2016; Wang et al., 2012). These stable and wet environmental conditions correspond with the globally recognized Mid-Piacenzian warm period between 3.3 – 3.0 Ma, and with the strengthening of the East Asian monsoon between 3.5 – 3.1 Ma (Qiang et al., 2001; Salzmann et al., 2011). Globally warm conditions coupled with local surges in precipitation may have produced the higher and more stable lake levels observed in the Qaidam Basin during this time (Qiang et al., 2001; Salzmann et al., 2011).

5.1.3 Unit 3A: 3.1 Ma – 3.0 Ma

Unit 3A consists of gypsum rich mudstone with interbedded gypsum layers, indicating a brief period of highly evaporitic conditions with sub-aqueous shallow playa lake deposition immediately following the wet conditions of Unit 2 (Figure 11A; Li et al,

2013). Sedimentation rates are at a maximum (~0.57 mm/yr) at this time, likely due to aeolian transportation of recently exposed near shore lacustrine sediments as the lake shoreline recedes back towards the shallowing depocenter at the QC section. Unit 3A shallow playa lake deposition transitions into Unit 3B shallow lacustrine deposition at ~3.0 Ma.

5.1.4 Unit 3B: 3.0 Ma – 2.7 Ma

Unit 3B consists mostly of mudstone with interlayered gypsum rich mudstone as well as gypsum beds (Figure 11A) and one distinct sandstone lens, indicating sub-aqueous shallow lacustrine deposition (Cooper, 1998; Pietras and Carroll, 2006). Sedimentation rates decrease to 0.22 mm/yr, which supports a slight deepening of the lake after Unit 3A (Figure 11B). However, the first appearance of limestone occurs at 267 m, just before a distinct ~20 cm fine sandstone lens with cross-trough bedding, both of which suggest shallow, near shore deposition (Miall, 2013; Pedley, 1990). Limestone deposition also indicates relatively low salinity and an increase in carbonate (Schreiber and Tabakh, 2000). The onset of this limestone deposition indicates a shift in the lake geochemistry likely due to a change in the relative position of the QC section within the lake or to a shift in sediment input from clastic to calcareous sediments (de Wet et al., 2016; Warren, 2010).

Throughout Unit 3, ~10 kyr cyclicity is recognized in the lake-level record (Figure 11C), indicating an unstable environment sensitive to short-term non-Milankovitch climatic cycles (Aref et al., 1997; Zachos et al., 2001). Cyclical amplification of events such as the East Asian monsoon can cause brief but intense surges in precipitation, which would, particularly in an arid setting, allow for brief mudstone

deposition, forming high frequency lake cycles within the sedimentological record (Yancheva et al., 2007; Qiang et al, 2001; Zachos et al., 2001).

The onset of limestone formation and the persistence of gypsum in the absence of halite indicate that deposition at the QC section is occurring in a shallow near-shore setting within a deeper lake that is potentially maintained by brief surges in precipitation (Schreiber and Tabakh, 2000; Warren, 2010). The depocenter of this lake therefore must have shifted, which could explain the lower sedimentation rates observed at the QC section (Figure 11B). Basin wide tectonic deformation uplifting a neighboring anticlinal formation at this time could account for this change in the position of the QC section, and it would be concurrent with ~3.0 Ma growth strata observed in the eastern Qaidam Basin (Heermance et al., 2013). However, investigation into the timing of uplift for the neighboring anticlinal formation is needed to test this hypothesis. Unit 3 is interpreted as gypsum rich shallow lacustrine deposition concurrent with a shift in the hydrogeologic setting (Figure 3B; Pietras and Carroll, 2006).

5.1.5 Unit 4: 2.7 Ma – ~1.7 Ma

The bottom of Unit 4 is marked by a dramatic increase in limestone deposition. Mudstone lithofacies continue to dominate the sedimentological record with interbedded gypsum rich mudstone, gypsum, and limestone as well as sandstone beds increasing in frequency upsection. Sedimentation rates remain low throughout Unit 4. Occasional stromatolite and oolite formation indicate a fluctuating shoreline at the location of the QC section, and a possible tufa bed suggests the potential initiation of local springs (de Wet et al., 2015; Fetter, 2000; Pedley 1990; Stauffer and Wittchen, 1991). The top of Unit 4 is

identified by a transition from mudstone to gypsum rich mudstone dominant lithofacies (Figure 11A).

After 2.5 Ma, $\delta^{18}O$ sampling resolution decreases; however two overall trends can be extrapolated from the low resolution isotope record: (1) slightly higher amplitudes suggesting more unstable conditions and (2) a slight trend towards more positive values, on average, indicating more evaporitic conditions (Jiang et al., 2008; Zachos et al., 2001). While these low resolution isotopic results are not definitive, they do indicate a trend towards more arid and unstable climatic conditions (Riebeek, 2005).

The increase of limestone deposition in Unit 4 indicates a continuation of the shifting hydrogeologic setting observed at the top of Unit 3, including an increase in the carbonate concentration and near-shore deposition at the QC section (Warren, 2010). Tectonic uplift of a neighboring anticlinal formation can account for a shifting shoreline at the QC section, and for the initiation of local springs (Fetter, 2000; Pedley, 1990; Stauffer and Wittchen, 1991). Unit 4 lithology is interpreted as a limestone and gypsum rich subaqueous near-shore setting of a deep and long-standing lake likely maintained by periodic surges in precipitation, while the oxygen isotope data indicates a trend towards more unstable and arid climatic conditions (Jiang et al., 2008; Schreiber and Tabakh, 2000; Warren, 2010).

5.1.6 Unit 5: ~1.7 Ma - ~1.5 Ma

Unit 5 (500 m – 540 m) begins with the major shift in lithology to gypsum rich mudstone dominated strata, with interbedded gypsum, limestone and sandstone, indicating a dramatic lake level drop (Li et al., 2013; Wang et al., 2012). The lack of

evaporite free siltstone deposition within the sedimentological record indicates that there are no periods of high lake levels (Ma et al., 2016). However, the lack of halite and of subaerial deposition and the presence of sandstone lithofacies indicate surface water input to the QC section throughout Unit 5, suggesting continuous subaqueous deposition (Jutras et al., 2007). Unit 5 is interpreted as deposition in a shallow subaqueous playa lake, indicating a trend towards more arid conditions, similar to the conditions found in the playa lakes of the Qaidam Basin today (Aref et al, 1997; Li et al, 2013).

5.1.7 After ~1.5 Ma

The remaining ~200 m (from 540 m - ~740 m) are inferred to be similar to the material observed in Unit 5. Most of this section is covered with a thick gypsum crust that limits direct sedimentological observation; however, this gypsum crust is likely the result of underlying gypsum-rich strata (Aref et al., 1997; Warren, 2010). This indicates a continued trend towards complete aridification through the Holocene, capped by the layer of active deposition at ~740 m in stratigraphic height (Kezao and Bowler, 1986).

5.2 Correlation to the QH Section

The QC section consists of fine-grained sediment deposited mostly offshore in a deep to shallow lake environment. The QH section, located ~100 km to the north of the QC section towards the margin of the basin, consists of coarser material with sedimentary structures indicating deposition in a high-energy shoreline environment (Figure 1A; Riegel, 2015).

Prior to 3.33 Ma, the QH section shows gypsum rich playa-fluvial active shoreline deposition while the QC section shows gypsum and halite rich playa lake deposition

(Figure 14, Figure 15A). At ~3.33 Ma, sedimentation in both the QH and QC sections transitions to deeper subaqueous deposition, indicating a basin wide response to the Mid-Piacenzian warm period (Figure 14; Figure 15B; Salzmann et al., 2011). After, 3.1 Ma, the QH section shifts from playa-lacustrine to playa-fluvial, while the QC section shifts from deep lacustrine to shallow lacustrine, both indicating lower lake levels and more arid conditions (Figure 15C). The onset of limestone deposition in the QC section at ~2.7 Ma is concurrent with the onset of calcareous sandstone deposition in the QH section, which may be due to additional concurrent lake shallowing events, or to the influx of calcareous lake sediments exposed by basin wide tectonic deformation (Figure 14). After ~2.5 Ma the QH section is interpreted as playa lake deposition, while the QC section is interpreted as near-shore deposition in a shallow lake with some passive shoreline deposition (Figure 15D). Both the QH and the QC sections indicate increasing aridification upsection after the mid-Piacenzian warm period.

The QC section and the QH section show relatively concurrent environmental transitions, both indicating the early onset of aridification, wet conditions during the Mid-Piacenzian warm period, and the Plio-Quaternary transition towards increasingly arid conditions (Salzmann et al., 2011; Zachos et al., 2001). There are three major differences between the sedimentology of these sections. First, the QH section represents active shoreline deposition while the QC section represents off-shore deposition to passive shoreline deposition. Second, at 2.7 Ma, the QH section contains calcareous sandstone while the QC section contains more defined limestone deposition. This may be due to (1) higher clastic sediment input from the surrounding mountains into the QH section lowering the relative amount of calcareous material in the brine at QH, or (2) that tectonic

deformation is occurring in closer proximity to the QC section, exhuming more calcareous sediment that is blown into the lake, increasing the relative amount of calcareous material in the brine at QC. Third, halite formation is observed throughout the QH section, but in the QC section, it is only observed prior to 3.33 Ma. The fluctuation between playa-fluvial and shallow playa lake deposition at the QH section maintains an environment conducive to halite formation. However, prior to 3.33 Ma is the only time when a shallow playa lake is present in the QC section that is conducive to halite deposition. After 3.33 Ma, the lake associated with the QC section remains relatively deep, likely with lower salinity. After 1.7 Ma, a shallow playa-lake depositional environment is present, but fresh surface water flow at the QC section during this time likely continues to prevent the formation of halite.

Together, these sections imply a large continuous lake present in the northwestern Qaidam Basin until ~2.7 Ma with offshore to nearshore lacustrine deposition in the QC section and shallow playa lake to active shoreline deposition in the QH section. After the initiation of limestone and calcareous sandstone deposition at 2.7 Ma, a general trend towards lower lake levels is observed in both sections, but the timing of sedimentological shifts are staggered, indicating the partitioning of this regional lake as well as increasingly arid conditions.

5.3 Proposed Reconstruction of the Qaidam Basin Climate Record (3.6 Ma – Today)

Initially, the QH section and the QC section were likely connected in one large regional lake (Kezao and Bowler, 1986; Wang et al., 2012). When aridification initiated, sometime before 3.6 Ma, this regional lake began to shrink (Figure 15A). However, these arid conditions were interrupted at ~3.33 Ma likely owing to increased precipitation

during the Mid-Piacenzian warm period, initiating high and more stable lake levels within the Qaidam Basin (Figure 15B; Qiang et al., 2001; Salzmann et al., 2011). By 3.1 Ma, the environment shifted back into more arid climatic conditions, causing the lake to shrink once again (Figure 15C). Continuous subaqueous deposition despite a shift towards more arid and evaporitic conditions after the mid-Piacenzian can be attributed to an increase in periodic precipitation owing to the strengthening of the East Asian monsoon (Qiang et al., 2001).

Evidence for tectonic deformation is observed within the Qaidam Basin at ~3.0 Ma (Heermance et al., 2013). If this deformation is due to basin wide tectonic activity, the hydrogeologic setting in the northwestern Qaidam Basin could be altered, potentially inducing the more calcareous deposition observed in both the QC and the QH sections. Uplift of a neighboring anticlinal formation could also change the relative location of the QC section within the lake from a distal depocenter to a nearshore setting. By ~2.7 Ma, the QC section was separated from the QH section, likely due to tectonic partitioning of the basin and a trend towards more evaporitic conditions (Figure 15D; Heermance et al., 2013). Surface water from the nearby mountains continued to recharge the QH section and transport some clastic sediment causing the formation of calcareous sandstone, and the shallow playa lake at the QH section was conducive to formation of both gypsum and halite (Riegel, 2015). Meanwhile, input of clastic sediments decreased in the QC section, causing precipitation of limestone. Although gypsum continued to form, hydrogeologic conditions did not favor halite formation in the QC section, possibly owing to deeper lake levels, lowering the salinity of the lake water (Schreiber and Tabakh, 2000).

After ~2.7 Ma, increased sandstone layers in the QC section indicate periodic precipitation and surface water flow, likely due to strengthening of the East Asian monsoon (Qiang et al., 2001). The lack of halite formation during the transition to a playa lake depositional environment is likely due to this increase in freshwater fluvial input at the QC section. The return to playa-fluvial material towards the top of the QH section also indicates increasing surface water flow around this time (Riegel, 2015). However, due to increased evaporitic conditions, the lake system continued to diminish despite periodic surges in precipitation (Figure 15E), forming highly gypsiferous sub-aqueous deposition. Eventually, the system shifted towards the hyper-arid conditions observed in the Qaidam Basin today (Figure 15F), which is consistent with the global cooling effects of the Plio-Quaternary transition (Wang et al., 2012; Zachos et al., 2001).

5.4 Climate Cyclicity

5.4.1 $\delta^{18}O$ Cyclicity in the Qaidam Basin

The stable isotopic record identifies dominant signals for both ~23 kyr precession cycles and ~100 kyr eccentricity cycles, although ~41 kyr obliquity cycles are also recognized (Figure 12A). Strong signals for both ~50 kyr cycles (a harmonic of the ~100 kyr cycle), and ~15 kyr cycles (a harmonic of the ~23 kyr cycle) further indicate the influence of eccentricity and precession (Zachos et al., 2001). Therefore, it is likely that climate cyclicity in the Qaidam Basin is dominated by ~23 kyr precession forcing, but it is modulated by ~100 kyr eccentricity forcing, consistent with the axial precession index (Ruddiman, 2008; Tziperman and Gildor, 2003).

5.4.2 Environmental Cyclicity in the Qaidam Basin

The frequency analysis for the timing of lake cycles is less conclusive, but it does recognize the influence of all three Milankovitch cycles: eccentricity, obliquity, and precession (Figure 12B). The largest deviation in the lake cycle frequency analysis compared to the $\delta^{18}O$ frequency analysis is the influence of short-term (<10 kyr) non-Milankovitch cycles. The abundance of these short-term cycles implies that the environmental response within this high elevation terrestrial setting is sensitive to small environmental perturbations. Cyclical brief intensification of events like the East Asian monsoon, particularly within this arid environment, could allow enough precipitation for thinly bedded lacustrine deposition (Qiang et al., 2001; Wang et al., 2008). Therefore, while the climatic record is driven by axial precession orbital forcing, the environmental record is influenced by orbital forcing, tectonic deformation and short-term climatic aberrations such as the East Asian monsoon (Wang et al., 2008; Zachos et al., 2001).

5.4.3 The Qaidam Basin Record vs. the Marine Record

Sedimentation in the Qaidam Basin seems to be a process restricted to interaction between the basin and its surrounding mountains which allows for a sedimentological record that is unique to this region (Wang et al., 2012; Zachos et al., 2001). The short term climatic cycle frequencies in the Qaidam Basin records from 3.6 – 1.7 Ma differ from the marine records for this time period. Benthic $\delta^{18}O$ records recognize ~23 kyr precession cycles, but identify the ~41 kyr obliquity cycle to be the dominant cycle period prior to 1.2 Ma (Lesiecki and Raymo, 2007). In contrast, these high-elevation terrestrial records recognize ~41 kyr obliquity cycle, but identify a ~100 kyr eccentricity

modulated ~23 kyr precession cycle as the dominant cycle frequency during this time (Figure 12).

Unlike the effects of obliquity forcing, the effects of precession forcing are minimal except when accentuated by eccentricity (Riebeek, 2006; Ruddiman, 2008). However, the Qaidam Basin may have an environment sensitive enough to consistently respond to the shorter period climatic cycles. This sensitivity may be attributed to a combination of high relief accentuating environmental fluctuations (i.e. formation of a rain shadow increasing aridity) and high elevation with a lack of vegetation augmenting surface exposure (Smith et al., 2013; Sun et al., 2008; Wang et al., 2012). In addition, the location of the Qaidam Basin (Latitude=37.7°) is within the range of influence from the Intertropical Convergence Zone (ITCZ), which triggers the millennial cycles of the East Asian monsoon (Yancheva et al., 2007). It is therefore possible that the Qaidam Basin is effected by obliquity forcing, but due to increased sensitivity, short-term cycles (i.e. precession as well as non-Milankovitch East Asian monsoon cycles) become more dominant in the record. Other areas with lower sensitivity might only recognize precession cycles when they are accentuated by eccentricity, and therefore identify obliquity as a more consistently dominant forcing mechanism.

Global climatic trends (i.e. the mid-Piacenzian warm period, or the onset of Northern Hemisphere glaciation driven by obliquity orbital forcing) still control the long term regional climatic trends for this high-elevation terrestrial setting (Salzmann et al., 2011; Ruddiman, 2008; Zachos et al., 2001). However, the short-term environmental response within the long-term trends is site-specific depending on many variables, possibly including the site location, elevation, relief, and vegetation.

6 CONCLUSION

The QC section spans ~740 m of Pliocene and Quaternary deposition. 182 paleomagnetic samples define 9 distinct magnetozones that correlate between 3.6 and 1.8 Ma (Gradstein et al., 2004). The lack of halite formation after 3.33 Ma and the onset of limestone formation at ~2.7 Ma in the QC section indicate a change in the brine geochemistry. This change may come from fluctuations in regional climate altering lake levels and lake shorelines as well as regional tectonic deformation partitioning the basin and shifting lake shorelines, changing the relative position of the QC section within the lake (de Wet et al., 2015; Heermance et al., 2013, Warren et al., 2010).

The stable isotopic and stratigraphic records from the QC section of the Qaidam Basin recognize global shifts in climate, such as the Mid-Piacenzian warm period from 3.33 Ma – 3.1 Ma, and the general trend towards more cold and arid icehouse conditions after the Plio-Quaternary boundary (Salzmann et al., 2011; Zachos et al, 2001). Similar trends are observed further north in the QH section, indicating a basin wide response to these global events. 65 lake-level cycles and 88 $\delta^{18}O$ climate cycles are recognized within the section, indicating frequent (axial precession and <10 kyr non-Milankovitch) cyclicity during the Pliocene and Pleistocene, which contradicts the marine record of ~41 kyr cycle dominance during this time (Lesiecki and Raymo, 2007; Zachos et al., 2001).

The results of this study indicate that, while climatic trends do seem to be globally consistent, short-term fluctuation in the terrestrial climate records can deviate from the marine climate record. The effects of orbital forcing are likely to be regionally variable depending on spatial variants (i.e. topography, elevation, or continentality). Global models must take these variables into account in order to more accurately predict the

short-term regional effects of global climate change. Continued research is necessary to further isolate the different variables that can influence the environmental sensitivity to different orbital forcing mechanisms in order to better understand the local short-term effects of global climate change.

REFERENCES

Aref, M.A.M., Attia, O.E.A. and Wali, A.M.A., 1997, *Facies and depositional environment of the Holocene evaporites in the Ras Shukeir area, Gulf of Suez, Egypt:* Sedimentary Geology, v. 110, p.123-145.

Bennett, M.R., Doyle, P. and Mather, A.E., 1996, *Dropstones: their origin and significance*: Palaeogeography, Palaeoclimatology, Palaeoecology, v. 121, p.331-339.

Berger, A., Loutre, M.F., Melice, J.L., 2006, *Equitorial insulation: from precession harmonics to eccentricity frequencies:* Climate of the Past: v. 2, p. 131-136.

Borradaile, G. J., Lucas, K., Middleton, R. S., 2004, *Low-temperature demagnetization isolates stable magnetic vector components in magnetite-bearing diabase:* Geophysical Journal International, v. 157, p. 526-536.

Brand, W. A., Coplen, T. B., Aerts-Bijma, A. T., Böhlke, J. K., Gehre, M., Geilmann, H., Gröning, M., Jansen, H. G., Meijer, H. A. J., Mroczkowski, S. J., Qi, H., Soergel, K., Stuart-Williams, H., Weise, S. M. and Werner, R. A., 2009, *Comprehensive inter-laboratory calibration of reference materials for δ18O versus VSMOW using various on-line high-temperature conversion technique*: Rapid Communication Mass Spectrometry, v. 23, p. 999–1019.

Casas, E. and Lowenstein, T.K., 1989, *Diagenesis of saline pan halite: comparison of petrographic features of modern, Quaternary and Permian halites*: Journal of sedimentary Research, v. 59.

Chen, J., Kravchinsky, V.A., Liu, X., 2015, *The 13 million year Cenozoic pulse of the Earth:* Earth and Planetary Science Letters, v. 431, p. 256-263.

Cody, R. D, Cody, A. M., 1988, *Gypsum Nucleation and Crystal Morphology in Analog Saline Terrestrial Environments*: SEPM Journal of Sedimentary Research SEPM JSR, v. 58, doi: 10.1306/212f8d69-2b24-11d7-8648000102c1865d.

Cooper, A. H., 1998, *Subsidence hazards caused by the dissolution of Permian gypsum in England: geology, investigation and remediation*: Geological Society, London, Engineering Geology Special Publications, v. 15, p. 265-275.

Craddock, William, Eric Kirby, and Huiping Zhang, 2011, *Late Miocene–Pliocene range growth in the interior of the northeastern Tibetan Plateau:* Lithosphere, p. 420-438.

de Wet, C. B., Godfrey, L., de Wet, A. P., 2015, *Sedimentology and stable isotopes from lacustrine-to-palustrine limestone deposited in an arid setting, climatic and tectonic factors: Miocene-Pliocene Opache Formation, Atacama Desert, Chile:* Palaeogeography, Palaeoclimatology, Palaeoecology, v. 426, p. 46-67.

Fang, X., Zhang, W., Meng, Q., Gao, J., Wang, X., King, J., Song, C., Dai, S., Miao, Y., 2007, *High-resolution magnetostratigraphy of the Neogene Huaitoutala section in the eastern Qaidam Basin on the NE Tibetan Plateau, Qinghain Province, China and its implications on tectonic uplift of the NE Tibetan Plateau:* Earth and Planetary Science Letters, v. 258, p. 293-306.

Fetter, C.W., 2000, *Applied hydrogeology*, Prentice hall.

Guo, X., Sun, Z., Lai, Z., Lu, Y., Li, X., 2015, *Optical dating of landslide-dammed lake deposits in the upper Yellow River, Qinghai – Tibetan Plateau, China*: Quaternary International, p. 1-6.

Gradstein, F. M., Ogg, J. G., Smith, A. G., Bleeker, W., & Lourens, L. J., 2004, *A new geologic time scale, with special reference to Precambrian and Neogene*: Episodes, v. 27, p. 83-100.

Heermance, R. V., Pullen, A., Kapp, P., Garzione, C. N., Bogue, S., Ding, L., Song, P., 2013, *Climatic and tectonic controls on sedimentation and erosion during the Pliocene-Quaternary in the Qaidam Basin (China)*: GSA Bulletin, v. 125, p. 833-856.

Jiang, H., Ji, J., Gao, L., Tang, Z., Ding, Z., 2008, *Cooling-driven climate change at 12-11 Ma: Multiproxy records from a long fluviolacustrine sequence at Guyuan, Ningxia, China:* Palaeogeography, Palaeoclimatology, Palaeoecology, v. 265, p. 148-158.

Jutras, P., Utting, J. and McLeod, J., 2007, *Link between long-lasting evaporitic basins and the development of thick and massive phreatic calcrete hardpans in the Mississippian Windsor and Percé groups of eastern Canada*: Sedimentary Geology, v. 201, p.75-92.

Kezao, C., Bowler, J.M., 1986, *Late Pleistocene evolution of salt lakes in the Qaidam Basin, Qinghai Province, China*: Paleogeography, Paleoclimatology, Paleoecology, v. 54, p. 87-104.

Kendall, C., Caldwell, E.A., 1998, *Fundamentals of Isotope Geochemistry: Chapter 2,* United States Geological Survey.

Kirschvink, J.L., 1980, *The least-squares line and plane and the analysis of palaeomagnetic data*: Geophysical Journal International, v. 62, p.699-718.

Leng, M.J. and Marshall, J.D., 2004, *Palaeoclimate interpretation of stable isotope data from lake sediment archives*: Quaternary Science Reviews, v. 23, p.811-831.

Lesiecki, L.E., Raymo, M.E., 2005, *A Pliocene-Pleistocene stack of 57 globally distributed benthic $\delta^{18}O$ records:* Paleoceanography: v. 20, p. 1-17.

Lesiecki, L.E., Raymo, M.E., 2007, *Plio-Pleistocene climate evolution: trends and transitions in glacial cycle dynamics*, Quaternary Science Reviews: v. 26, p. 56-69.

Li, M., Fang, X., Wang, J., Song, Y., Yang, Y., Zhang, W., Liu, X., 2013, *Evaporite minerals of the lower 538.5 m sediments in a long core from the Western Qaidam Basin, Tibet*: Quaternary International, v. 298, p. 123-133.

Liu, X., Sun, H., Miao, Y., Dong, B., Yin, Z., 2015, *Impacts of uplift of northern Tibetan Plateau and formation of Asian inland desert on regional climate and environment:* Quaternary Science Reviews, v. 116, p. 1-14.

Lowenstein, T.K. and Risacher, F., 2009, *Closed basin brine evolution and the influence of Ca–Cl inflow waters: Death Valley and Bristol Dry Lake California, Qaidam Basin, China, and Salar de Atacama, Chile*: Aquatic Geochemistry, v. 15, p.71-94.

Ma, Y., Fan, M., Lu, Y., Liu, H., Hao, Y., Xie, Z., Liu, Z., Peng, L., Du, X. and Hu, H., 2016, *Climate-driven paleolimnological change controls lacustrine mudstone depositional process and organic matter accumulation: Constraints from lithofacies and geochemical studies in the Zhanhua Depression, eastern China*: International Journal of Coal Geology, v. 167, p.103-118.

Magee, J.W., Bowler, J.M., Miller, G.H. and Williams, D.L.G., 1995, *Stratigraphy, sedimentology, chronology and palaeohydrology of Quaternary lacustrine deposits at Madigan Gulf, Lake Eyre, South Australia*: Palaeogeography, Palaeoclimatology, Palaeoecology, v. 113, p.3-42.

McClung, W.S., Eriksson, K.A., Terry, D.O., Cuffey, C.A., 2013, *Sequence stratigraphic hierarchy of the Upper Devonian Foreknobs Formation, central Appalachian Basin, USA: Evidence for transitional greenhouse to icehouse conditions*: Paleogeography, Paleoclimatology, Paleoecology, v. 387, p. 104-125.

McFadden, P.L. and McElhinny, M.W., 1990, *Classification of the reversal test in palaeomagnetism*: Geophysical Journal International, v. 103, p.725-729.

Miall, A., 2013, *The geology of fluvial deposits: sedimentary facies, basin analysis, and petroleum geology*. Springer.

Moy, C.M., Seltzer, G.O., Rodbell, D.T. and Anderson, D.M., 2002, *Variability of El Niño/Southern Oscillation activity at millennial timescales during the Holocene epoch*: Nature, v. 420, p.162-165.

Opdyke, N.D., Channell, J.E.T., 1996, *Magnetic Stratigraphy: Laboratory Techniques*, Academic Press Inc., v. 64, p. 49-61

Pedley, H.M., 1990, *Classification and environmental models of cool freshwater tufas*: Sedimentary Geology, v. 68, p.143-154.

Pietras, J. T., Carroll, A. R., 2006, *High-resolution stratigraphy of an underfilled lake basin: Wilkins Peak Member, Eocene Green River Formation, Wyoming, U.S.A:* Journal of Sedimentary Research, v. 76, p. 1197-1214.

Qiang, X. K., Li, Z. X., Powell, C. M., Zheng, H. B., 2001, *Magnetostratigraphic record of the Late Miocene onset of the East Asian monsoon, and Pliocene uplift of northern Tibet*: Earth and Planetary Science Letters, v. 187, p. 83-93.

Raymo, M. E., Ruddiman, W. F., 1992, *Tectonic forcing of late Cenozoic climate:* Nature, v. 359, p. 117-122.

Riebeek, H., 2005, *Paleoclimatology: the oxygen ballence*, NASA Earth Observatory: http://earthobservatory.nasa.gov/Features/Paleoclimatology_OxygenBalance/

Riegel, H.B., 2015, *Magnetostratigraphic analysis of Late Miocene-Pliocene strata in the northwestern Qaidam Basin, China* (Unpublished Master's Thesis), California State University Northridge, Northridge, CA, USA.

Riegel, H.B., Heermance, R.V., Nie, J., Su, Q., Garzione, C.N., 2015, *Lake-level fluctuation and climate cyclicity observed in lake strata in the northwestern Qaidam Basin, China* (Abstract), AGU Fall Meeting: 12/14/2015 – 12/18/2015.

Rohrmann, A., Heermance, R.V., Kapp, P., Cai, F., 2013, *Wind as the primary driver of erosion in the Qaidam Basin, China:* Earth and Planetary Science Letters, v. 374, p. 1-10.

Ruddiman, W.F., 2008, Earth's *Climate Past and Future: Second Edition:* W.H. Freeman and Company, p 116 – 203.

Saadeh, C.M., Saylor, J.E., Shanahan, T.M., Nie, J., 2015, *Mid-Pliocene onset of eccentricity cycles in the Zhada Basin, southwestern Tibetan Plateau* (Abstract), AGU Fall Meeting: 12/14/2015 – 12/18/2015.

Salzmann, U., Williams, M., Haywood, A.M., Johnson, A.L.A., Kender, S., Zalasiewicz, J., 2011, *Climate and environment of a Pliocene warm world*, Palaeogeography, Palaeoclimatology: Palaeoecology, v. 309, p. 1-8.

Smith, P., Ashmore, M. R., Black, H. I., Burgess, P. J., Evans, C. D., Quine, T. A., Thompson, A. M., Hicks, K., Orr, H. G., 2013, *The role of ecosystems and their management in regulating climate, and soil, water and air quality*: Journal of Applied Ecology, v. 50, p. 812-829.

Stauffer, R.E. and Wittchen, B.D., 1991, *Effects of silicate weathering on water chemistry in forested, upland, felsic terrane of the USA*: Geochimica et Cosmochimica Acta, v. 55, p.3253-3271.

Sun, J., Zhang, L., Deng, C., & Zhu, R., 2008, *Evidence for enhanced aridity in the Tarim Basin of China since 5.3 Ma:* Quaternary Science Reviews, v. 27, p. 1012-1023.

Tziperman, E., Gildor, H., 2003, *On the mid-Pleistocene transition to 100-kyr glacial cycles and the asymmetry between glaciation and deglaciation times:* Paleoceanography, v. 18, p. 1-8.

Wang, X., Qui, Z., Li, Q., Wang, B., Qui, Z., Downs, W.R., Xie, G., Xie, J., Deng, T., Takeuchi, G.T., Tseng, Z.J., Chang, M., Liu, J., Wang, Y., Biasatti, D., Sun, Z., Fang, X., Meng, Q., 2007, *Vertebrate paleontology, biostratigraphy, geochronology, and paleoenvironment of Qaidam Basin in northern Tibetan Plateau*: Paleogeography, Paleoclimatology, Paleoecology, v. 254, p. 363-385.

Wang, Y., Zheng, J., Zhang, W., Li, S., Liu, X., Yang, X, Liu, Y., 2012, *Cenozoic uplift of the Tibetan Plateau: Evidence from the tectonic-sedimentary evolution of the western Qaidam Basin:* Geoscience Frontiers, v. 3, p. 175-187.

Wang, Y., Cheng, H., Edwards, R. L., Kong, X., Shao, X., Chen, S., Wu, J., Jiang, X., Wang, X., An, Z., 2008, *Millennial-and orbital-scale changes in the East Asian monsoon over the past 224,000 years:* Nature, v. 451, p. 1090-1093.

Yancheva, G., Nowaczyk, N. R., Mingram, J., Dulski, P., Schettler, G., Negendank, J. F., Liu, J., Sigman, D. M., Peterson, L. C., Haug, G. H., 2007, *Influence of the intertropical convergence zone on the East Asian monsoon*: Nature, v. 445, p. 74-77.

Zachos, J., Pagani, M., Sloan, L., Thomas, E., Billups, K., 2001, *Trends, Rhythms, and Aberrations in Global Climate 65 Ma to Present*, Science: v. 292, p. 686-693.

Zhang, G., Yao, T., Xie, H., Wang, W., Yang, W., 2015, *An inventory of glacial lakes in the Third Pole region and their changes in response to global warming:* Global and Planetary Change, v. 131, p. 148-157.

Zhang, W., Appel, E., Fang, X., Yan, M., Song, C., Cao, L., 2012, *Paleoclimatic implications of magnetic susceptibility in Late Pliocene-Quaternary sediments from deep drilling core SG-1 in the western Qaidam Basin (NE Tibetan Plateau)*: Journal of Geophysical Research, v. 117, p. 1-16.

APPENDIX A:

FIGURES

Figure 1

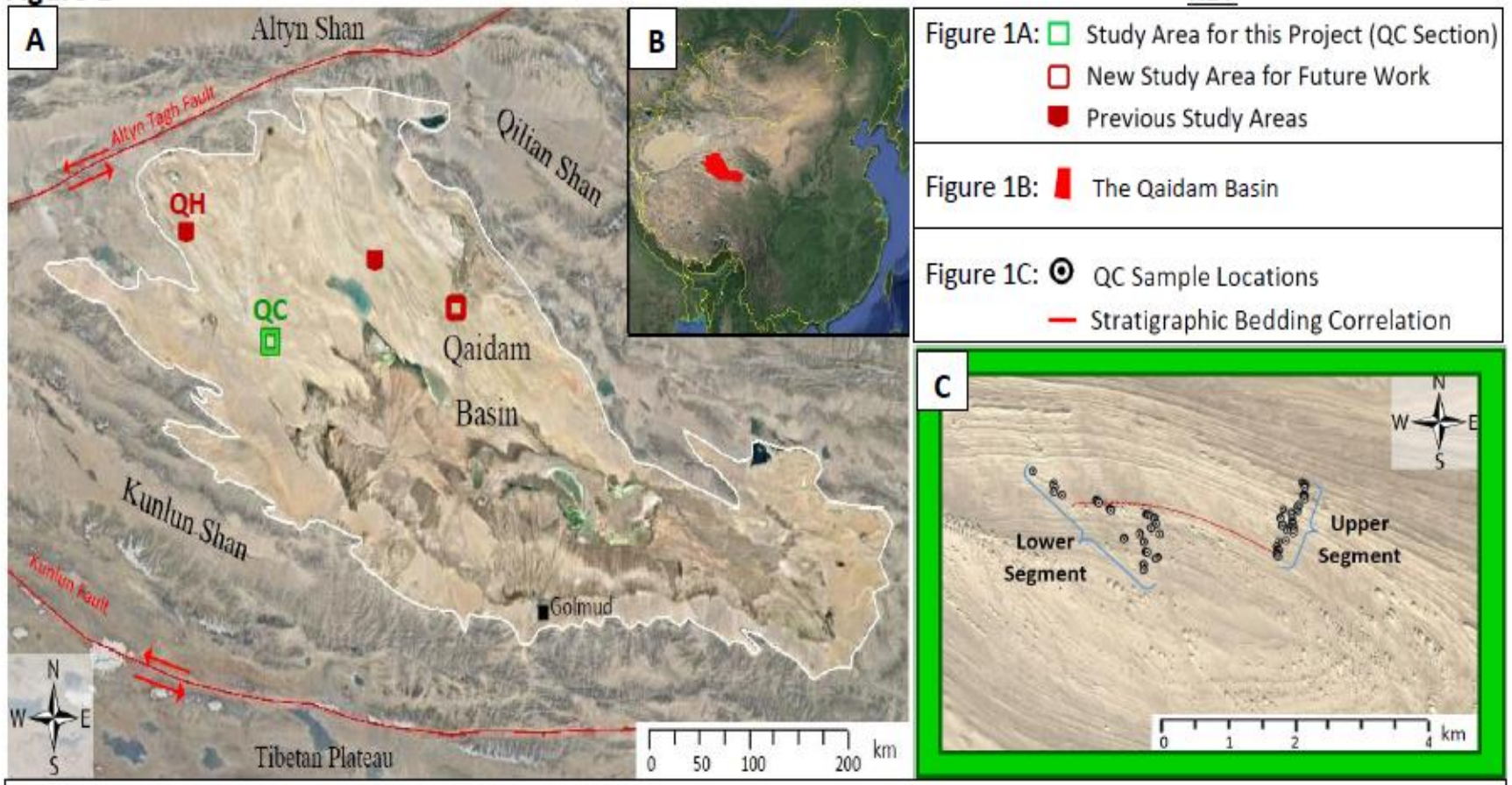

Figure 1: (A) A satellite image of the Qaidam Basin showing major faults and mountain ranges surrounding the basin, previous and future study areas marked in red, and the current study area (the QC section) marked in green. Karst topography is observed in the mountains north of Golmud. (B) A context map showing the location of the Qaidam Basin in the northeastern margin of the Tibetan Plateau. (C) A closer look at the QC section with a satellite image showing the sample locations and their distribution between the lower segment (0 m – 226 m in stratigraphic height) and the upper segment (201 m – 477 m in stratigraphic height) of the stratigraphic section.

Figure 2

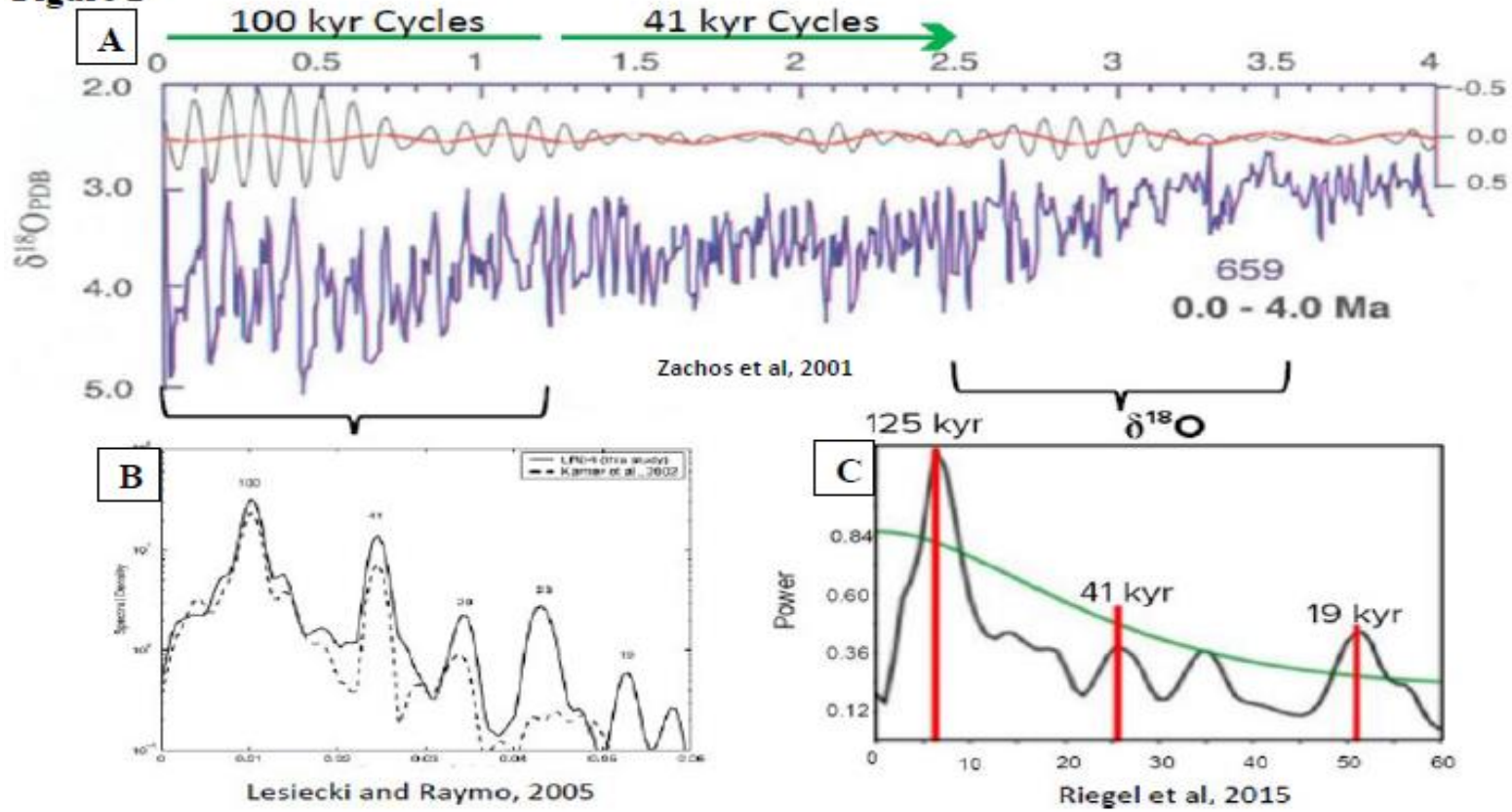

Figure 2: Compiled $\delta^{18}O$ data and analyses for the last 4 million years. (A) The benthic $\delta^{18}O$ record from Zachos et al (2001) shows the general cooling trend associated with the Plio-Quaternary transition. (B) The frequency plot from Lesiecki and Raymo (2005) of the same benthic record indicates that the climate has fluctuated on 100 kyr eccentricity cycles since ~1.2 Ma. Prior to this, the climate record was dominated by 41 kyr obliquity cycles (Lesiecki and Raymo, 2007). (C) The frequency plot from Riegel et al (2015) was produced using terrestrial $\delta^{18}O$ data, and it indicates that the 41 kyr signal is the weakest signal, and that the terrestrial climate record is dominated by 100 kyr eccentricity cycles before the Plio-Quaternary boundary, contradicting the marine record.

Figure 3

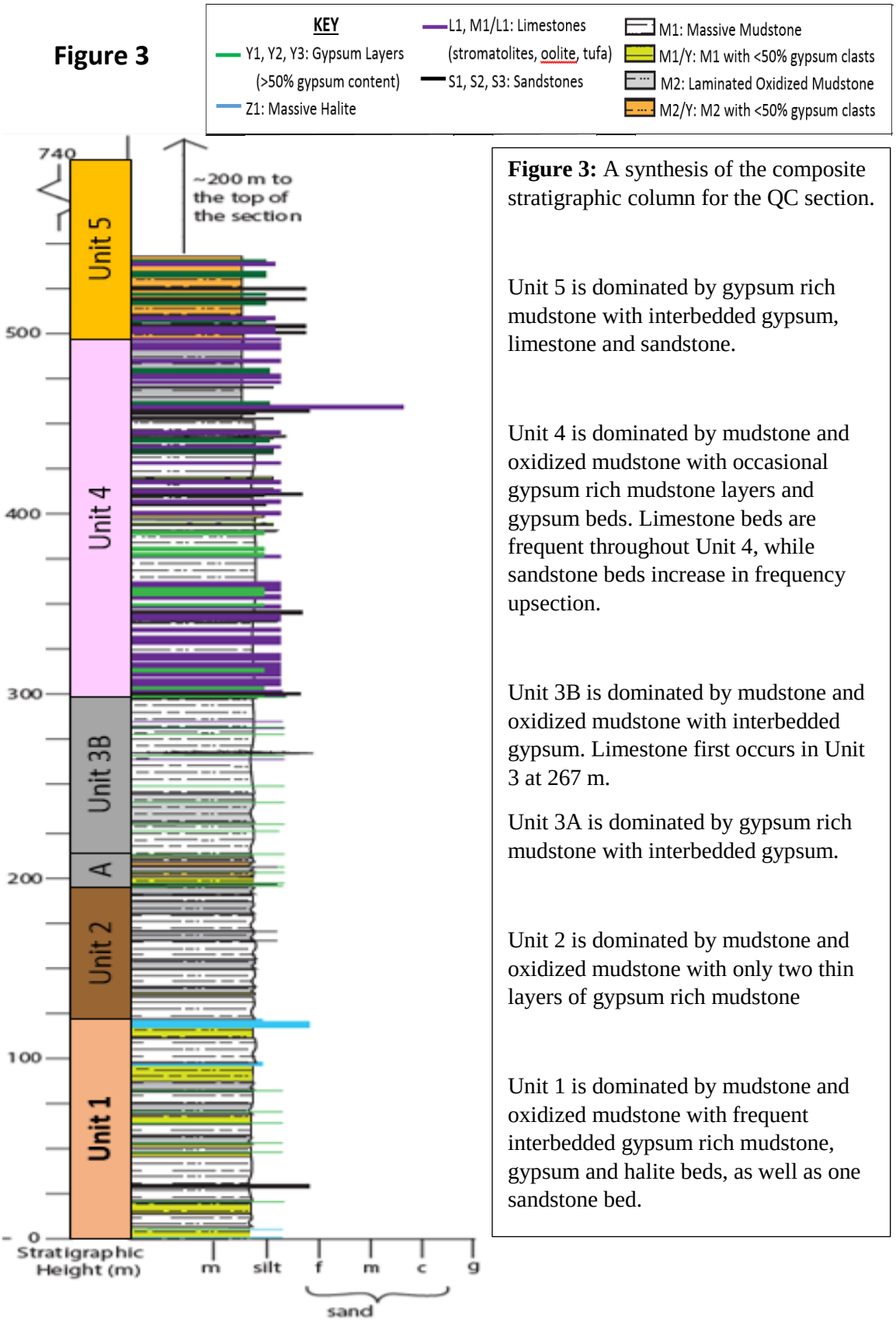

Figure 3: A synthesis of the composite stratigraphic column for the QC section.

Unit 5 is dominated by gypsum rich mudstone with interbedded gypsum, limestone and sandstone.

Unit 4 is dominated by mudstone and oxidized mudstone with occasional gypsum rich mudstone layers and gypsum beds. Limestone beds are frequent throughout Unit 4, while sandstone beds increase in frequency upsection.

Unit 3B is dominated by mudstone and oxidized mudstone with interbedded gypsum. Limestone first occurs in Unit 3 at 267 m.

Unit 3A is dominated by gypsum rich mudstone with interbedded gypsum.

Unit 2 is dominated by mudstone and oxidized mudstone with only two thin layers of gypsum rich mudstone

Unit 1 is dominated by mudstone and oxidized mudstone with frequent interbedded gypsum rich mudstone, gypsum and halite beds, as well as one sandstone bed.

Figure 4

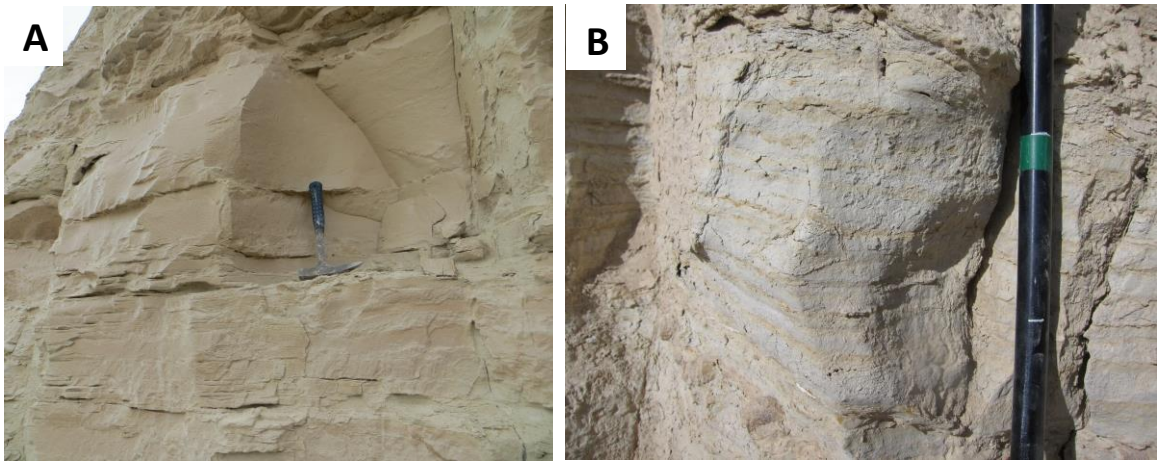

Figure 4: Photographs of mudstone facies from field work in the QC section. (A) M1: a yellowish grey (5Y 7/2) siltstone which weathers to a brownish pink color. Photo taken by Lin Li at 125 m in stratigraphic height within the lower segment of the QC section. (B) M2: a mottled light brownish grey (5YR 6/1) siltstone with interbedded 1 mm oxidized deposits that range from red to orange-brown in color. Photo taken by Richard Heermance at 213.5 m in the upper segment of the QC section

Figure 5

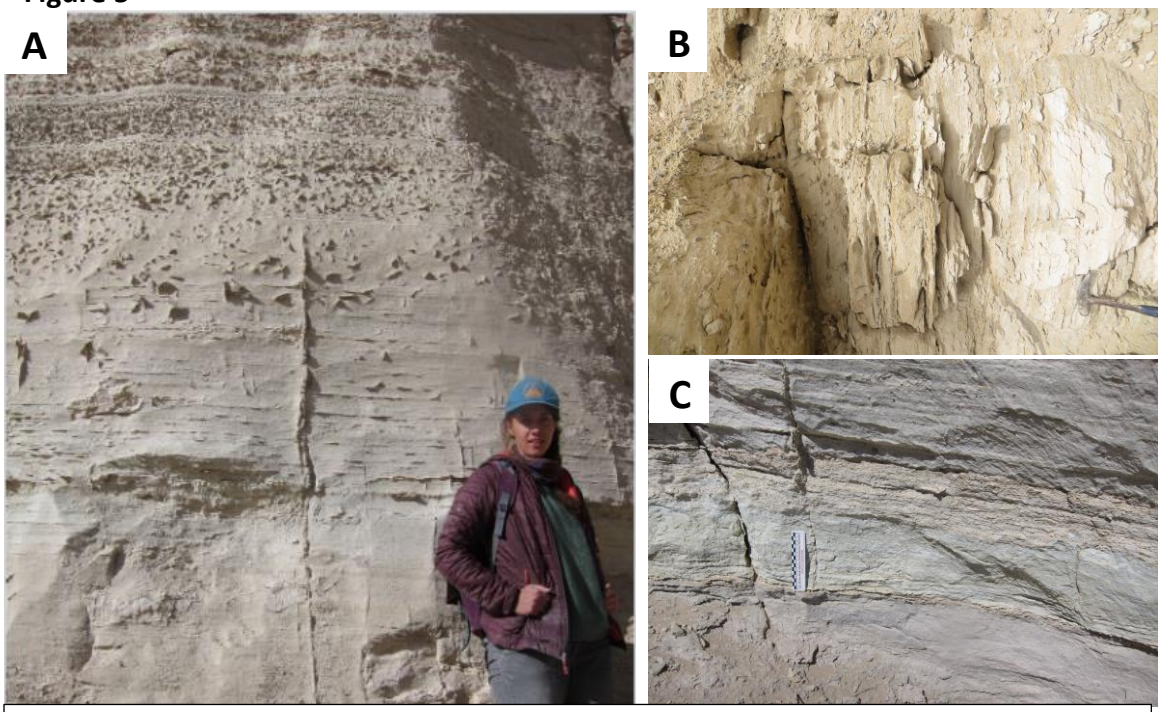

Figure 5: Photographs of evaporite rich mudstones from field work in the QC section. (A) M1/Y: an M1 layer that contains chipped gypsum crystals. Photo taken by Richard Heermance at 214 m - 217 m. (B) M2/Y: an M2 layer that contains chipped gypsum crystals. Photo taken by Lin Li at 209 m. (C) M3: mottled yellow (10Y 8/3) siltstone that contains minor amounts of gypsum. Photo taken by Richard Heermance at 438 m.

Figure 6

Figure 6: Photographs of evaporite layers from field work in the QC section. (A) Y1: a siltstone layer with 50 % milky white gypsum crystals; photograph taken at 45 m in stratigraphic height. (B) Y2: microcrystalline gypsum layer; photograph taken at 19 m in stratigraphic height. (C) Z1: hardpan halite layer; photograph taken at 4 m in stratigraphic height. All photographs were taken by Lin Li.

Figure 7

Figure 7: A photograph of stromatolite L1: a medium – dark grey (N1) calcareous limestone. Photo taken by Richard Heermance at 312 m in stratigraphic height. L1 is also observed as tufa, oolite and lamination within thicker M1 bedding. L1 strata occasionally form hogback ridges. Limestone first occurs at 267 m, and becomes more frequent above 300 m.

Figure 8

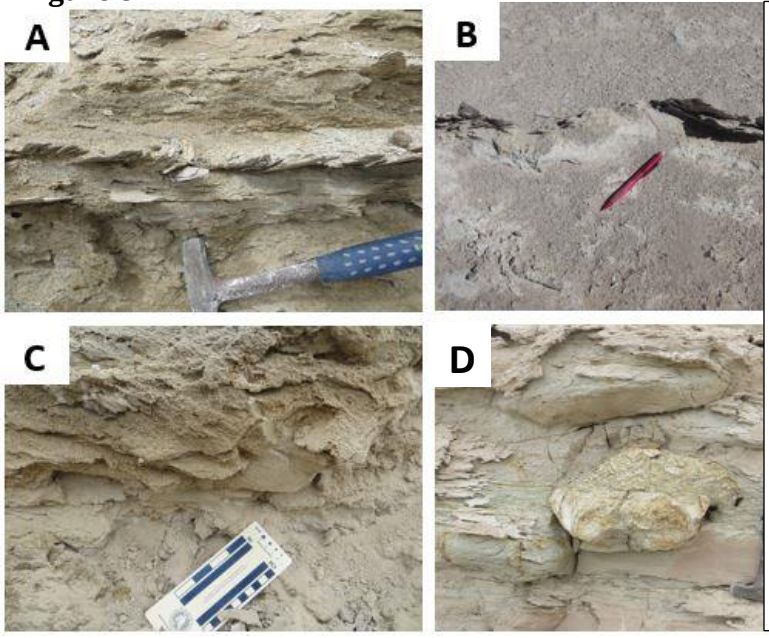

Figure 8: Photographs of sandstone lithofacies from field work in the QC section. (A) S1: a fine sandstone with trough-cross bedding. Photo taken by Lin Li at 40 m. (B) S2: pale orange fine sandstone with a hummocky contact. Photo taken by Richard Heermance at 304.5 m. (C) S3: a thin discontinuous lens of fine calcareous sandstone. Photo taken by Lin Li at 28 m. (D) an in situ sandstone dropstone. Photo taken by Lin Li at 53.5 m.

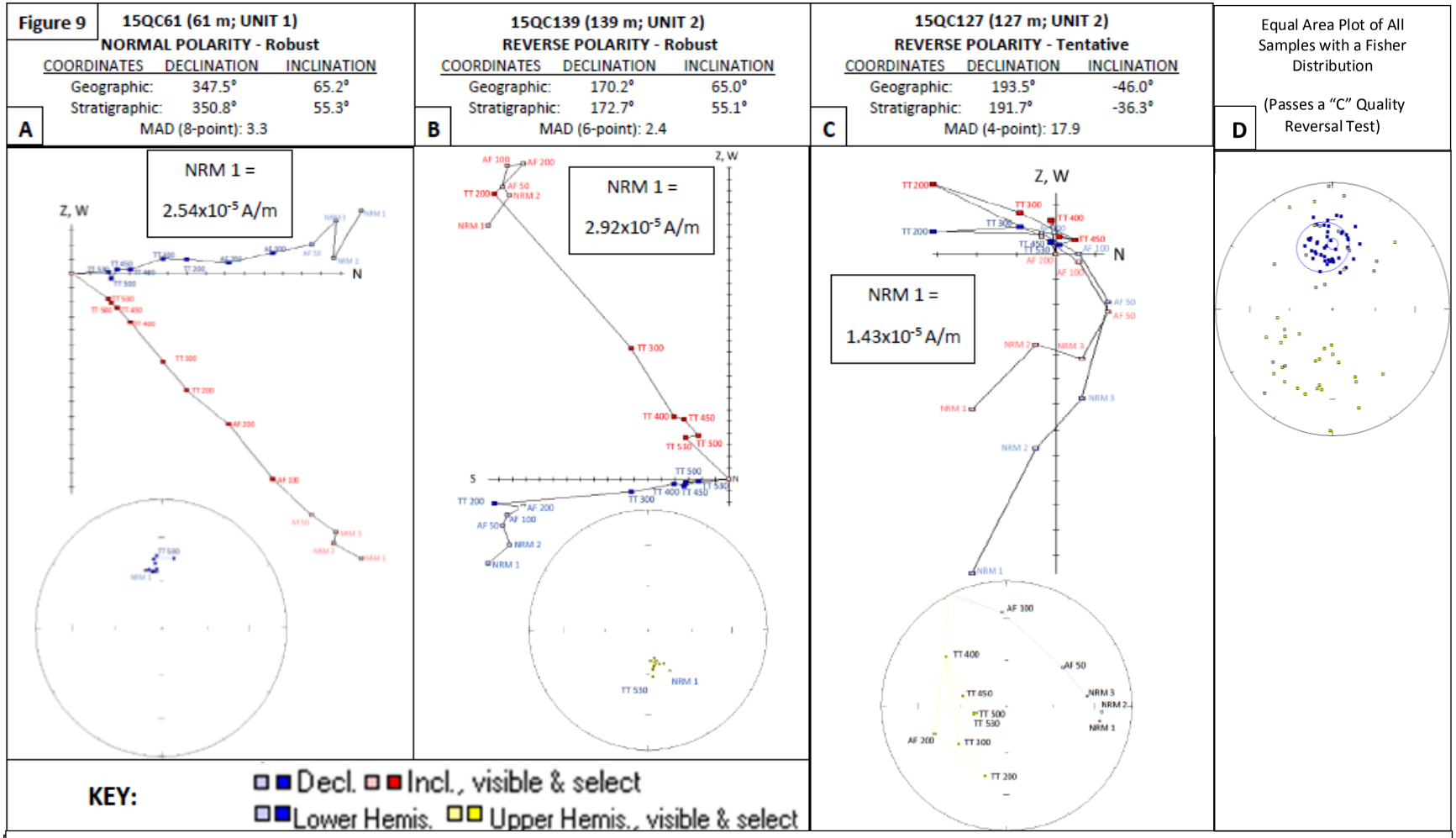

Figure 9: Examples of paleomagnetic analysis using orthographic and equal area plots (Kirschvink, 1980). Initial Natural Remnant Magnetization (NRM) values are listed for each sample. AF is Alternating Field demagnetization. TT is Thermal demagnetization. (A) Sample 15QC61 shows a robust Normal signal. (B) Sample 15QC139 shows a robust Reverse signal. (C) Sample 15QC127 shows a tentative Reverse signal. (D) Equal area plot for all paleomagnetic data with a Fisher Distribution (blue circle).

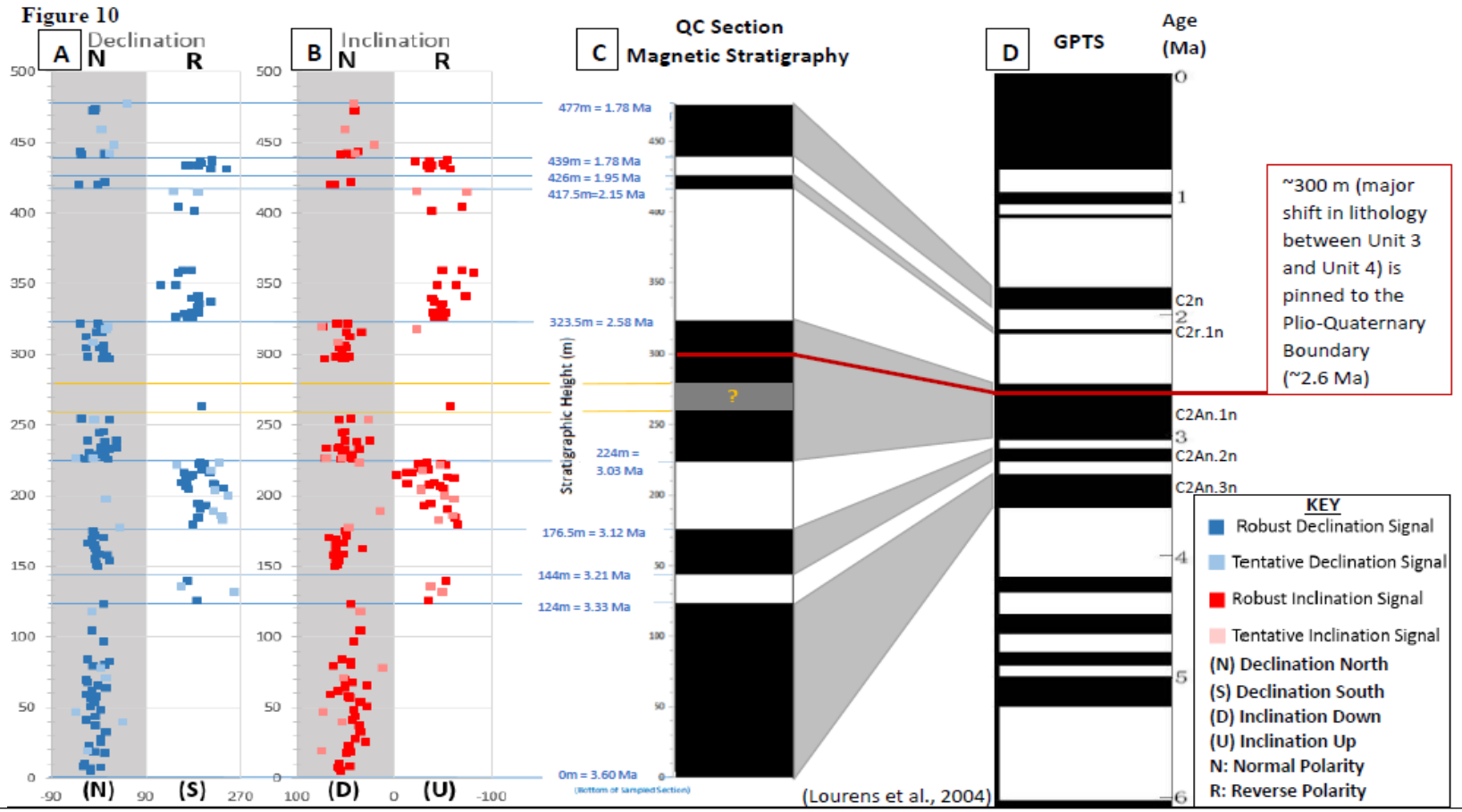

Figure 10: Samples showing tentative and robust paleomagnetic signals have been graphed by declination (A) and inclination (B) on the x-axis vs. stratigraphic height on the y-axis. In (A) and (B), samples that fall within the grey shaded region show normal polarity, while the samples that fall within the unshaded region show reverse polarity. Grouping samples by polarity produces the magnetic stratigraphic record of the QC section (C)). Exact stratigraphic height for each magnetic reversal event is identified in blue. A single sample at ~265 m shows reverse polarity, but the potential for error is too high with a single sample, so this potential magnetozone is not used in this study. A total of 9 distinct magnetozones are identified within the QC section, which correlate to the GPTS (D) between 3.6 Ma and 1.8 Ma (Lourens et al.,

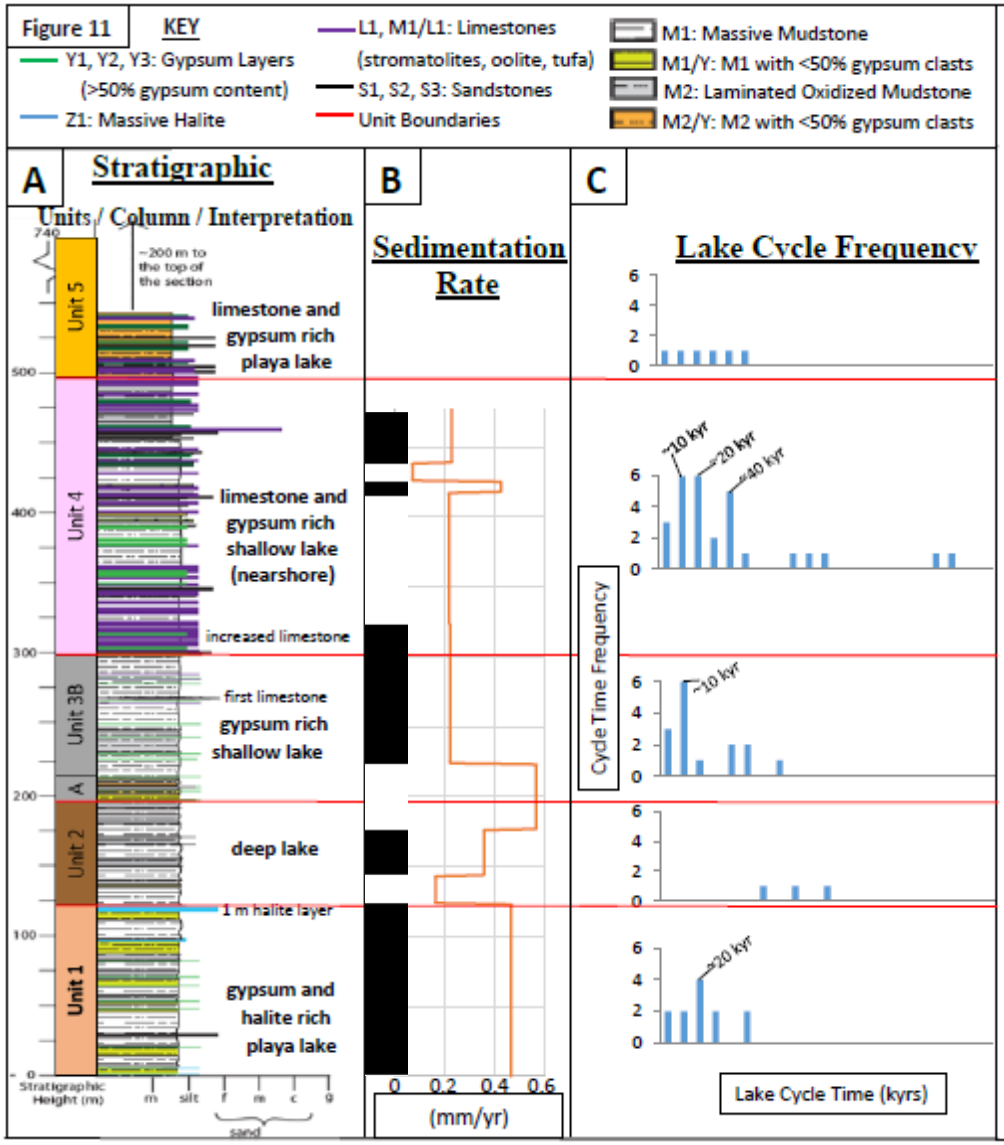

Figure 11: The sedimentological record for the QC section of the Qaidam Basin. (A) The composite stratigraphic column with stratigraphic units and interpretations, (B) calculated sedimentation rates, and (C) lake cycle frequencies for each stratigraphic unit.

Unit 5: High evaporite content and short period (<55 kyr) lake level cyclicity indicate a playa lake.

Unit 4: Gypsum content and relatively low sedimentation rates (~0.2 mm/yr) indicate some level of aridity. Frequent limestone indicates a significant change in the water chemistry. Lake cyclicity is variable (2 kyrs – 177 kyrs). This indicates a nearshore lacustrine setting.

Unit 3: Mudstone and gypsum, low sedimentation rates and short (<15 kyr) cyclicity indicates a shallow lacustrine setting.

Unit 2: A lack of evaporitic material indicates a deep lacustrine setting.

Unit 1: Mudstone, gypsum and halite, high sedimentation rates and shorter (~20 kyrs) lake cycle times indicate a surface water fed playa lake setting.

Figure 12

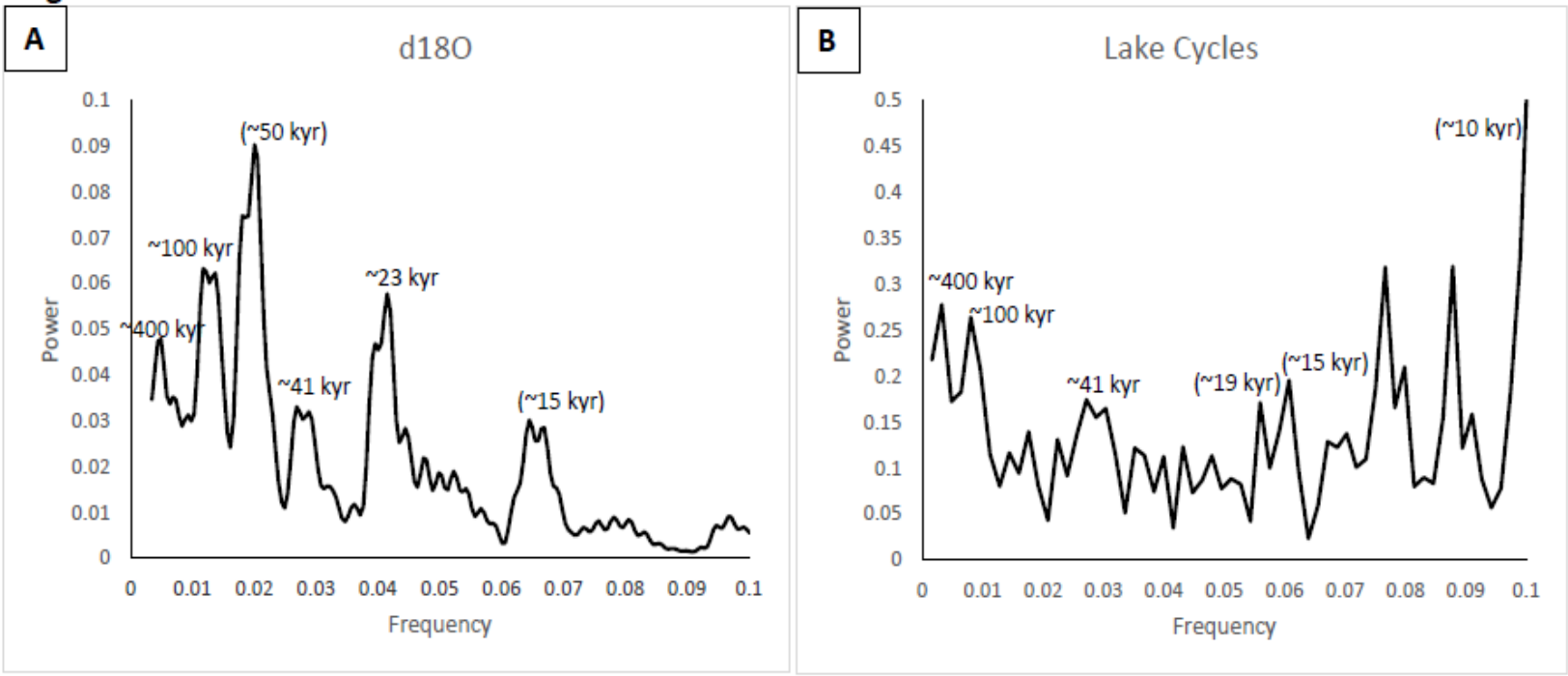

Figure 12: The δ18O frequency plot (A) shows that ~100 kyr (eccentricity) and ~23 kyr (precession) cycles are dominant, indicating a dominant signature for axial precession in the oxygen isotopic data. The ~50 kyr signal is a harmonic of the eccentricity signal, and the ~15 kyr signal is a harmonic of the ~23 kyr signal. Strong signals for both the ~15 and the ~50 kyr cycle support axial precession dominance. The 41 kyr (obliquity) cycle is also recognized in the oxygen isotope data. The lake cycle frequency plot (B) indicates a high occurrence of short-term (<15 kyr) non-milankovich lake level cycles. There are also peaks for showing the influence of precession, obliquity and eccentricity.

Figure 13

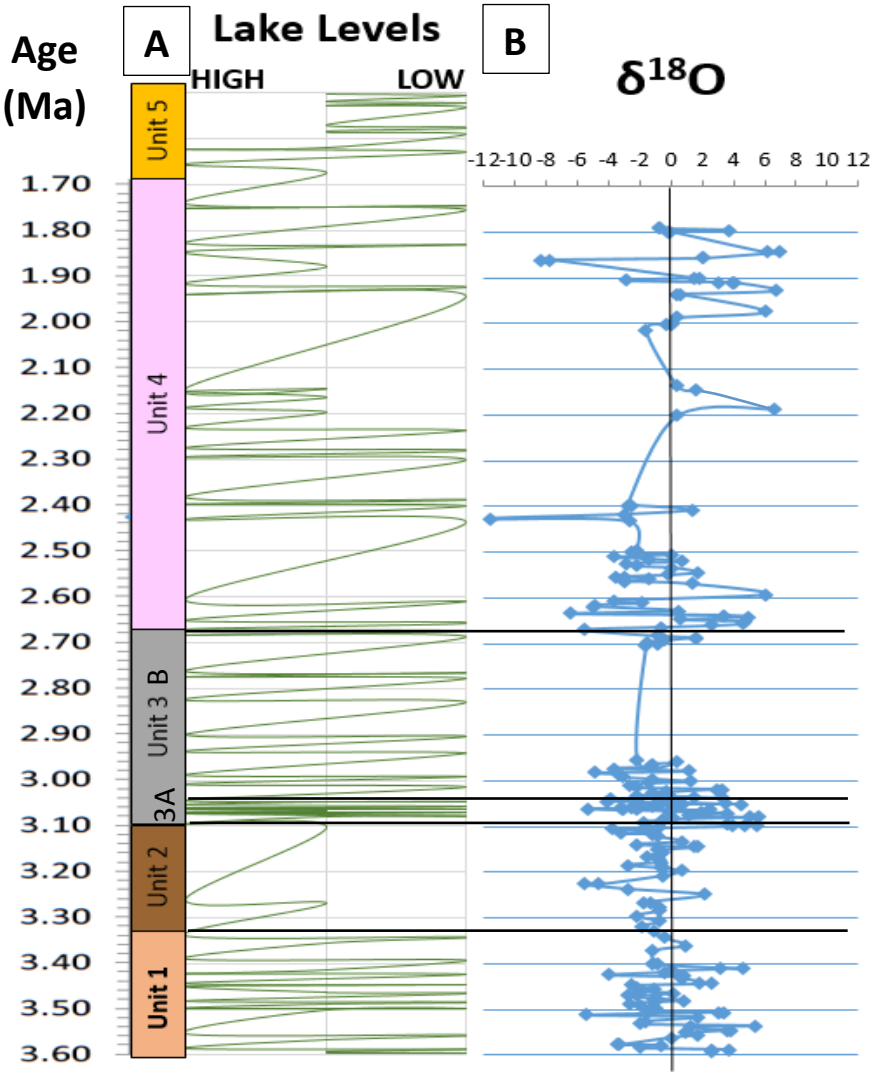

Figure 13: Compiled stratigraphic and stable isotopic data for the QC section with corresponding ages, shown to the left, representing millions of years ago (Ma). (A) Stratigraphic Units 1-5 (left) are aligned with lake level cyclicity, shown in green (right). The isotope graph shows $\delta^{18}O$ data in blue (B). Results of the $\delta^{18}O$ data support the environmental conditions seen in the stratigraphic record. Data for the $\delta^{18}O$ record indicate a trend towards more cold and arid conditions approaching the top of the sampled section, just before hyper-arid conditions are observed in the stratigraphic record.

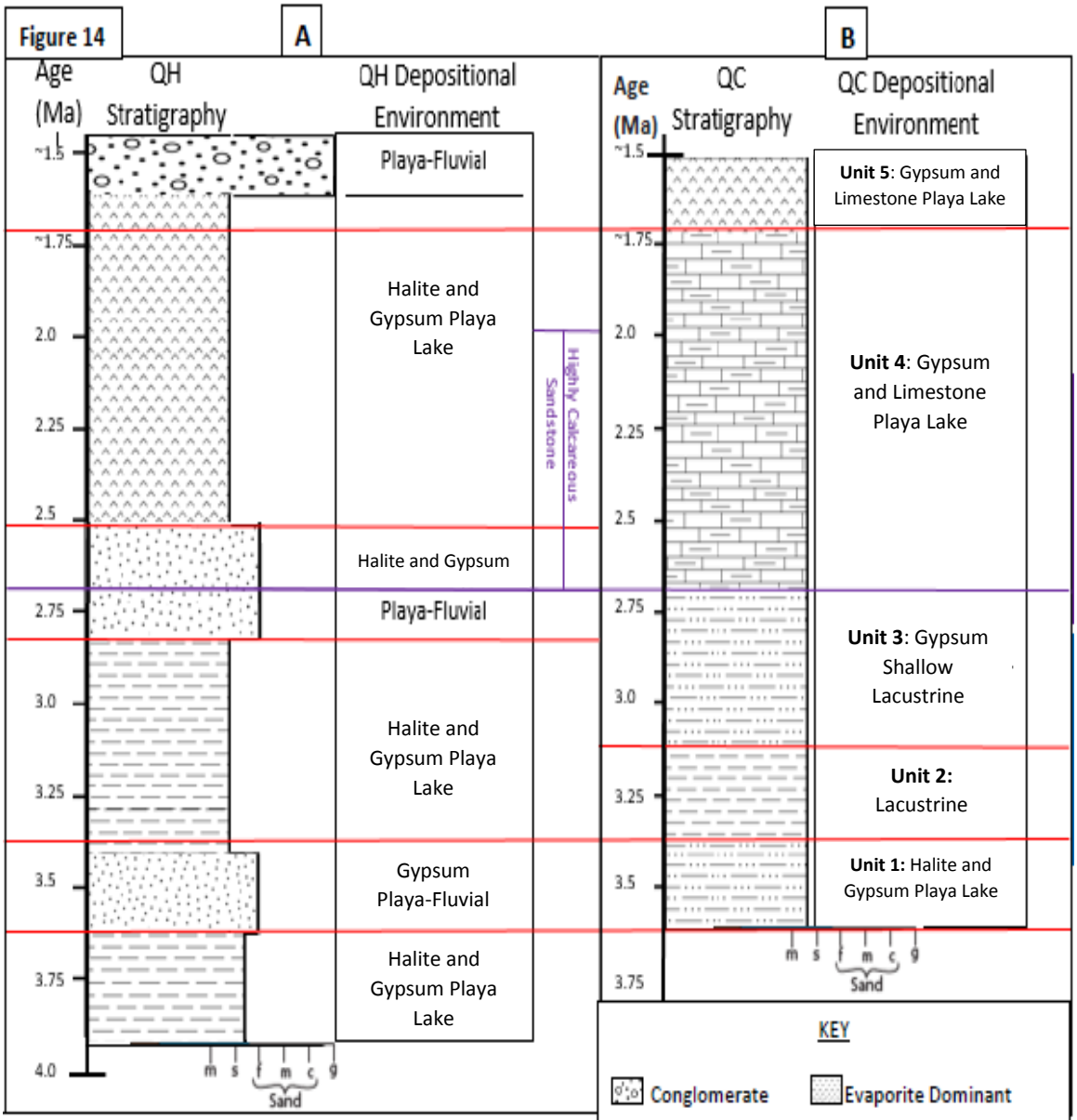

Figure 14: Correlation between the QH section (an active shoreline depositional environment located in the northwestern margin of the Qaidam Basin), and the QC section (a low-energy playa-lacustrine depositional setting located in the northwestern Qaidam Basin). These sections are ~60 km apart. The stratigraphic columns show the most characteristic lithofacies of each stratigraphic unit.

Figure 15

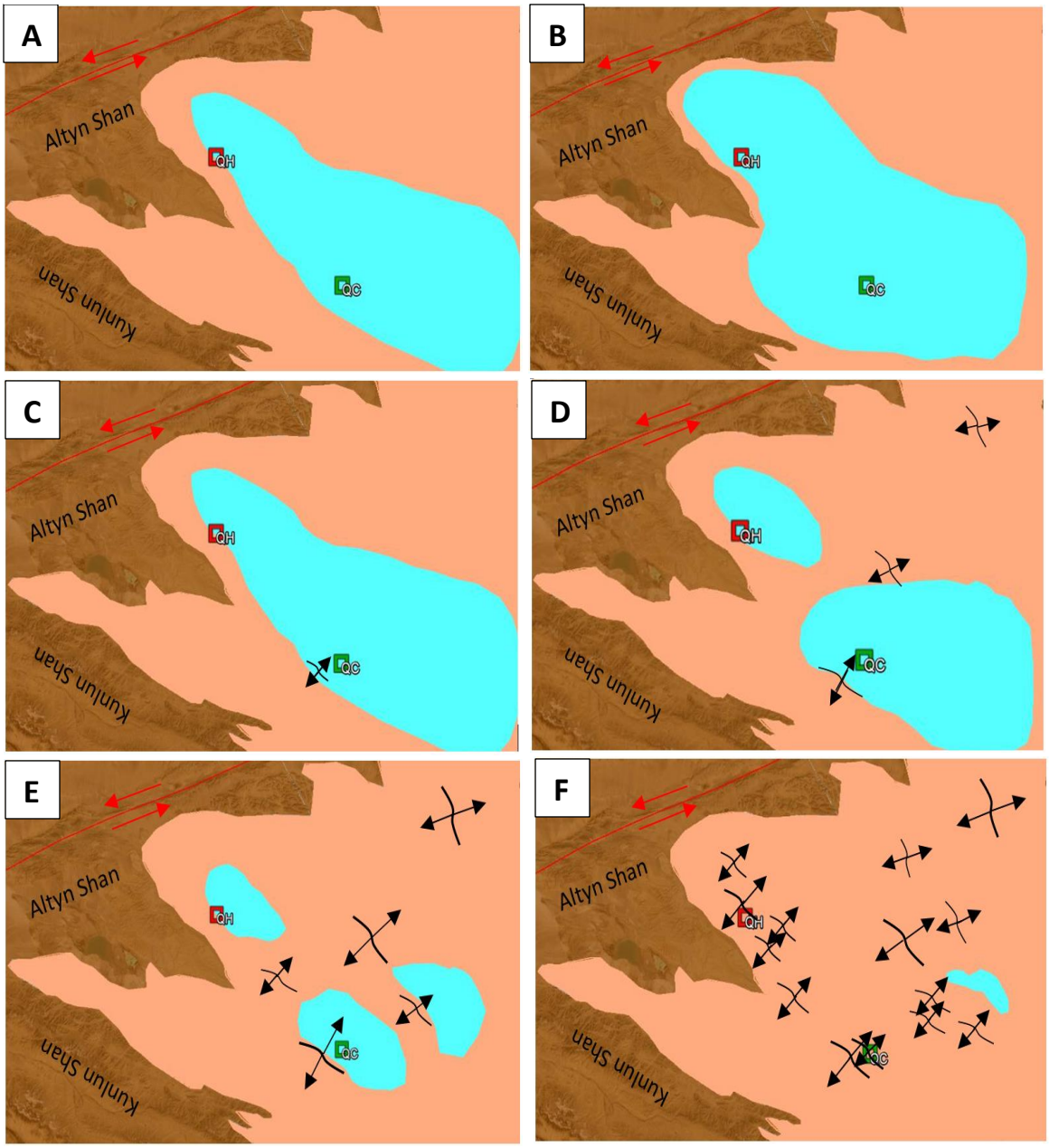

Figure 15: A paleogeographic interpretation for the Qaidam Basin from 3.6 Ma through today. (A) 3.6 Ma – 3.33 Ma: early onset of aridification. (B) 3.33 Ma – 3.1 Ma: wetter conditions during the mid-Piacenzian warm period. (C) 3.1 Ma – 2.7 Ma: a return to more arid conditions and the onset of regional tectonic deformation, shifting the hydrogeologic setting around the QC section. (D) 2.7 Ma – 1.7 Ma: A continued trend towards more arid conditions as the lake system dwindles. Uplift of an anticlinal formation close to the QC section causes partitioning of the basin, a shifting shoreline at the QC section, limestone deposition, and potentially the formation of springs. (E) After 1.7 Ma: increasing evaporitic content as the lake system continues to dwindle. (F) Today: tectonically deformed and wind-eroded hyper-arid basin with very few highly saline playa lakes.

APPENDIX B:

TABLES

Table 1: Lithofacies Chart

Lithofacies Unit ID	Lithofacies Description			Lithofacies Interpretation
	Grain Size / Color	Bedding	Geometry	
Mudstones				
M1	silt (0.004 mm - 0.063 mm) yellowish grey (5Y 7/2)	total range: 1 m - 15 m most common range: 2 m - 5 m massive bedding	laterally continuous	deep lacustrine depostion wet climate
M2	silt (0.004 mm - 0.063 mm) mottled light brownish grey (5YR 6/1)	total range: 1 m - 10 m most common range: 2 m - 4 m 0.1 cm - 2.0 cm horizontal lamination	laterally continuous	deep lacustrine depostion wet climate
Gypsum Rich Mudstones				
M1/Y	silt (0.004 mm - 0.063 mm) yellowish grey (5Y 7/2) <50% milky white - translucent gypsum crystals	total range: 1 m - 10 m most common range: 2 m - 4 m massive bedding	laterally continuous	shallow lacustrine deposition semi-arid climate
M2/Y	silt (0.004 mm - 0.063 mm) mottled light brownish grey (5YR 6/1) <50% milky white - translucent gypsum crystals	total range: 0.5 m - 7 m most common range: 1 m - 3 m 0.1 cm - 2.0 cm horizontal lamination	laterally continuous	shallow lacustrine deposition semi-arid climate
M3	silt (0.004 mm - 0.063 mm) mottled yellow (10Y 8/3) 5% - 10% microcrystalline gypsum	total range: 0.5 m - 2 m most common: 1 m 0.1 cm - 2.0 cm horizontal lamination	laterally continuous	shallow lacustrine deposition semi-arid climate
Evaporites				
Y1	silt (0.004 mm - 0.063 mm) greyish orange (10YR 7/4) >50% milky white - translucent gypsum crystals	total range: 10 cm - 50 cm most common: 20 cm	laterally continuous	shallow playa lake deposition arid climate
Y2	silt (0.004 mm - 0.063 mm) >50% microcrystalline gypsum	most common: 10 cm	laterally continuous	shallow playa lake deposition arid climate
Y3	yellowish grey (5Y 7/2) ~100% hardpan gypsum	total range: 5 cm - 10 cm	laterally continuous	shallow playa deposition hyperarid climate
Z1	bluish grey (5BG 5/1) ~100% hardpan halite	total range: 0.02 m - 1.0 m most common: 5 cm - 10 cm	laterally continuous	shallow playa deposition hyperarid climate
Limestone				
L1	medium - dark grey (N1) calcareous	total range: 1 cm - 10 cm	laterally continuous	lacustrine deposition semi-arid climate
M1/L1	Interbedded M1 and L1 layers	M1: 10 cm - 30 cm L1: 1 cm - 10 cm	laterally continuous	lacustrine deposition semi-arid climate
Sandstone				
S1	fine sand (0.125 mm - 0.250 mm)	total range: 10 cm - 20 cm	trough-cross bedding	fluvial deposition shift in lake margin; surface water input
S2	pale orange fine sand (0.125 mm - 0.250 mm)	most common: ~3 cm	laterally discontinuous hummocky contact	fluvial deposition shift in lake margin; surface water input
S3	fine sand (0.125 mm - 0.250 mm) calcareous	total range: 2 cm - 5 cm	laterally discontinuous	fluvial deposition shift in lake margin; surface water input

Table 2: Stratigraphic Units

Stratigraphic Unit	Stratigraphic Height (m)	Lithologic Description	Environmental Interpretation
Unit 5	500 - 540	Dominated by M2/Y with frequent interlayered L1, Y1, Y2, S1, S2 and S3 beds.	The setting shifts to a shallow playa lake dominated environment, with continued limestone deposition.
Unit 4	300 - 500	Dominated by M1 and M2, with frequent interlayered M1/Y, Y1, and Y2 beds that are increasing in both thickness and frequency up-section. Abbrupt increase in L1 and M1/L1 throughout the unit.	A distinct shift in water chemistry occurs at the boundary between Units 3 and 4, pursisting throughout the remaining section. The setting has returned to an arid environment with inconsistent lake desiccation cycles. Shifting hydrogeology indicates that groundwater input has increased, and surface water input has decreased.
Unit 3B	217 - 300	Dominated by M1 and M2 with interlayered Y1, Y2 and M1/Y beds. First appearance of infrequent L1 beds.	The short period of arid conditions is followed by a longer period of semi-arid conditions with some lake desiccation cycles. A shift in the hydrogeologic setting initiates here, with the onset of limestone deposition.
Unit 3A	185 - 217	Diminated by M1/Y and M2/Y interlayered with relatively thin M1 and M2 beds, and Y1 and Y2 beds.	A short period of arid conditions immediatealy follows the long warm/wet peroid in Unit 2.
Unit 2	120 - 185	Sharp transition from Z1 bed to M1. Dominated by M1 and M2 (except for 2 short [~5m] intervals of M1/Y)	The arid playa setting (Z1 at the top of Unit 1) is flooded as climate shifts back to wet conditions. Aridification is inturrupted by long wet period with high standing lake levels.
Unit 1	0 - 120	Dominated by M1 and M2, with frequent interlayered M1/Y, Y1 and Z1 beds with one S1 bed and 1 fine sandstone dropstone. Unit 1 is capped by thick Z1 bed	The onset of aridification has already occurred, showing multiple lake desiccation cycles with increasing aridity up-section and a distinct arid period identified by the Z1 cap layer. Halite indicates surface water input.

Table 3: Paleomagnetic Data

Sample	Stratigraphic Height (m)	Polarity	Geologic		Stratigraphic			# of data points used	MAD
			declination	inclination	declination	adjusted declination	inclination		
1QC276	477	n	63.3	48.4	56.3	56.3	40	6	8.9
QC273	474	N	356.8	49.2	357.3	-2.7	39.2	8	8.1
QC271A	472	N	352.5	49.9	353.8	-6.2	39.9	8	13.1
QC271B	472	N	352	49	353.3	-6.7	39	7	6.5
1QC258A	459	N	5.3	59.6	8.6	8.6	48.8	4	3.2
1QC258B	459	N	2	60.1	6.1	6.1	49.5	4	4.4
1QC247	448	n	32	29.3	31.1	31.1	18.5	6	3.5
QC242	443	N	323.5	44	328.2	-31.8	35.7	9	5.4
1QC241A	442	n	25.5	49.6	24.5	24.5	38.7	5	2.1
1QC241B	442	N	13.8	57.3	15	15	46.4	8	7.6
QC240A	441	N	319.6	60.9	328.7	-31.3	52.7	6	11.9
QC240B	441	N	18.2	52.6	15	15	43	5	15.2
QC236	437	R	230	-64.1	217.7	217.7	-56.9	8	10.8
QC235	436	r	221.4	-30.9	218.2	218.2	-23.2	9	4.9
1QC235	436	r	195.6	-48	196.3	196.3	-36.9	6	13.9
QC234	435	R	205.6	-61.9	199.6	199.6	-52.7	9	5.4
QC232	433	R	193.8	-50.5	191.6	191.6	-40.7	9	2.4
1QC232A	433	R	166.1	-62.7	174.7	174.7	-53	6	11.2
1QC232B	433	R	164.8	-44.9	169.8	169.8	-35.5	5	13.1
QC230A	431	R	222.7	-45.4	217	217	-37.8	8	10.3
QC230B	431	R	262.1	-61.2	245.5	245.5	-58.4	5	16.2
1QC220	421	N	12.6	53.1	14	14	42.1	5	8
QC219A	420	N	312.7	67.1	325.8	-34.2	59.5	9	5.5
QC219B	420	N	1.7	74.2	1.1	1.1	64.2	6	1
1QC214	415	r	140.4	-30.5	145.2	145.2	-24.5	5	10.9
QC213.5	414.5	R	215.4	-85.6	190.7	190.7	-76.2	9	7.2
1QC203	404	R	118.6	-76.6	153.7	153.7	-71.5	7	2.3
QC200	401	R	185.8	-49.6	184.9	184.9	-39.6	9	3.9
1QC158A	359	R	156.9	-81.4	178.4	178.4	-71.5	7	2.8
1QC158B	359	R	151.9	-59.7	161.9	161.9	-51.1	7	5.9
QC156	357	R	33.1	-85.1	155.5	155.5	-83.5	10	5.1
1QC148A	349	R	124.9	-72	149.6	149.6	-66.1	6	8.7
1QC148B	349	R	109.2	-47	120.5	120.5	-45.2	7	9.1
QC140	341	R	213.2	-84.7	191.4	191.4	-75.3	10	2.5
QC138A	339	R	177.7	-50.8	180.5	180.5	-41.1	10	4.2
QC138B	339	R	186.2	-50.5	185.2	185.2	-40.5	6	3.7
QC136	337	R	219.5	-52.7	215.3	215.3	-43.4	10	1.4
QC134	335	R	193.8	-61.6	194.1	194.1	-50.6	10	4.2
QC132	333	R	194.1	-58.9	191.1	191.1	-49.1	11	3.8
QC128	329	R	183.1	-66.3	186.7	186.7	-55.5	8	2.7
1QC128A	329	R	190.5	-52.7	191.4	191.4	-41.7	6	3.4
1QC128B	329	R	174.1	-54.7	178.5	178.5	-44.3	6	3.8
QC127A	328	R	155.3	-56.8	163.6	163.6	-47.7	8	3.6
1QC125A	326	R	177.1	-60.1	181.5	181.5	-49.6	6	5.7
1QC125B	326	R	137.1	-59	149.8	149.8	-52.1	6	11.7
QC125C	326	R	169.1	-52.6	171	171	-42.8	6	1.1
QC120A	321	N	317	65.6	328.3	-31.7	57.6	10	6.1
QC120B	321	N	0.8	56.8	0.7	0.7	46.8	6	12.2
QC118A	319	n	49.2	81.5	22.8	22.8	73.2	9	11.2
QC118B	319	N	13.2	81.7	5.9	5.9	71.9	6	13.9
QC116	317	N	14.6	-14.3	15.6	15.6	-23.9	8	3.6
QC114	315	N	11	57.7	8.8	8.8	47.9	8	2.9
1QC114A	315	N	280.3	31.9	0	0	32.2	7	2
1QC114B	315	N	155.6	23.9	0	0	32.1	7	3.1
QC111	312	N	335.6	53.8	340	-20	44.5	8	8.9
QC107	308	N	349.8	65.6	352.5	-7.5	55.6	8	16.7
QC105	306	N	15.8	58.3	12.5	12.5	48.7	9	15.1
QC103A	304	N	333.3	56.7	338.6	-21.4	47.6	9	3.6
QC103B	304	N	5.6	64.9	4.2	4.2	55	7	9.6
QC99	300	N	16.1	61.8	12.2	12.2	52.1	10	3.1
QC97	298	N	21.5	55.1	17.4	17.4	45.7	10	9.2
1QC107	296	N	16.6	81.8	16.1	16.1	70.8	7	3.6
QC95	296	N	11.1	59.2	8.7	8.7	49.3	6	12.4
15QC6-3	288	N	336.4	67.7	343.2	-16.8	58.4	10	5.3
15QC6-1	287	N	29.3	60.3	22.9	22.9	51.3	8	10.8
15QC5-1A	266	R	225.9	-69.9	211.8	211.8	-62	7	6.3
15QC5-1B	263	R	205.3	-67.6	198	198	-58.3	8	9.7
15QC4-2	254	N	323.9	51.3	329.8	-30.2	43	8	7.2
1QC52	253	n	350.9	35.1	354.3	-5.7	25.8	3	14.3
15QC4-1A	253	N	30.4	63.4	22.9	22.9	54.5	7	12.8
15QC4-1B	253	N	30.4	63.4	22.9	22.9	54.5	7	12.8
15QC3-2	246	N	15.5	59.1	12.1	12.1	49.4	9	4.4
15QC3-1	245	N	6.1	61.8	4.6	4.6	51.9	10	4.3
1QC37.5A	238.5	N	40.8	58.6	36.5	36.5	49.1	6	1.8
1QC37.5B	238.5	N	338.3	31	341.6	-18.4	23.4	7	3.8
QC37	238	N	12.2	47.2	13.4	13.4	37.3	11	8

Sample	Stratigraphic Height (m)	Polarity	Geologic		Stratigraphic			# of data points used	MAD
			declination	inclination	declination	adjusted declination	inclination		
QC35	236	N	326.7	60.4	338.1	-21.9	53.6	11	6
15QC2-2	236	N	9.4	64.5	7	7	54.6	9	8.8
QC33	234	N	4.2	64.5	8.3	8.3	54.8	11	3.4
15QC2-1	234	n	26.6	43.9	23.1	23.1	34.8	8	13.1
1QC32	233	N	50.3	77.5	37.5	37.5	68.3	9	2.5
QC32	233	N	29.9	65.1	27.3	27.3	55.2	11	4.8
QC31	232	N	11.1	59.1	13	13	49.1	11	6
QC29	230	N	335	59.1	344.4	-15.6	51.5	11	12.5
QC27A	228	N	342.7	49.8	348.5	-11.5	41.6	9	6.3
QC27B	228	N	352.6	50.8	357.1	-2.9	41.8	7	7.5
15QC1-4	227	N	17.8	56.3	14.3	14.3	46.6	10	5.3
QC25	226	N	296.6	73	324.3	-35.7	69.3	8	11.6
1QC25A	226	N	306.4	56.2	319.3	-40.7	52.4	9	3.9
1QC25B	226	N	333.5	75.3	351.8	-8.2	67.3	6	15.5
15QC226	226	N	336.6	50.8	340.4	-19.6	41.5	6	4.5
15QC1-3	224	N	29.7	62.3	22.7	22.7	53.3	9	14.2
15QC224	224	r	225.9	28.1	230.6	230.6	34.7	5	27.2
15QC1-2	223	R	198.3	-44.8	195.8	195.8	-35.2	10	13.7
QC21	222	R	194.8	-36.2	195.3	195.3	-26.3	9	3.6
15QC222	222	R	205.7	-63.6	199.4	199.4	-54.4	6	10.4
15QC1-1	222	R	209.5	-57.9	203.4	203.4	-49	6	2.6
1QC20	221	R	142.8	-54.4	152.8	152.8	-48.3	5	16.4
15QC220	220	R	201.9	-39.2	199.3	199.3	-30	6	8.1
QC17	218	R	199.6	-45.8	199.6	199.6	-35.8	9	3.2
15QC218	218	r	220.1	-38.4	215.7	215.7	-30.4	6	34
QC15	216	r	215.7	-24.8	214.8	214.8	-15.1	9	13.3
15QC216	216	R	162.6	-29.5	163.9	163.9	-20	6	7
15QC214	214	R	181.1	-14.8	181.1	181.1	-4.7	6	19.4
QC11	212	R	169.3	-64.6	177.2	177.2	-55.7	8	9.8
QC10	211	R	155	-70.5	169.3	169.3	-62.6	6	10.1
15QC209	209	r	155.8	-51.7	159.9	159.9	-42.4	7	33.9
QC7	208	r	222.1	-24.8	220.7	220.7	-15.5	7	6.4
15QC207	207	R	229.2	-44.1	223	223	-37.2	6	9.7
QC5	206	R	163.7	-56.2	170.7	170.7	-47.8	6	15.4
15QC205	205	R	255	-56	242.1	242.1	-52.3	6	7.3
QC3	204	R	172.4	-39.1	175.5	175.5	-30.1	4	12.8
15QC203	203	r	229.4	-36.3	224.7	224.7	-29.4	6	12.5
15QC199	199	r	262.2	-56.3	248.5	248.5	-53.8	4	15.3
15QC197	197	R	13.3	-53.5	17.8	17.8	-63.2	3	17.4
15QC194	194	R	192.5	-48.8	190.6	190.6	-39	6	8.3
15QC192	192	R	208.8	-40.5	205.4	205.4	-31.6	6	3.5
15QC190	190	R	201.7	-65.8	195.9	195.9	-56.4	6	1.4
15QC188	188	r	219.9	5.7	221.3	221.3	13.3	5	39.8
15QC185	185	r	254.4	-66.2	235.6	235.6	-61.9	5	14.4
15QC184	184	R	199.2	-73.6	192.2	192.2	-64	5	6.6
15QC182	182	R	249.6	-51.7	239	239	-47.4	5	14.1
15QC181	181	n	348.2	-23.2	347	-13	-32.9	6	27.3
15QC179	179	R	182.9	-77	181.7	181.7	-67	5	9
15QC177	177	n	53.7	52.2	45	45	45.8	5	6.9
15QC174	174	N	350	59.5	352.1	-7.9	49.6	6	2.7
15QC171	171	N	352.4	58.3	354	-6	48.3	6	7.2
15QC170	170	N	21.4	75.3	13	13	65.8	6	5.7
15QC168	168	N	346.4	68	350.4	-9.6	58.2	5	5.8
15QC166	166	N	336.5	59.9	341.7	-18.3	50.6	5	7.3
15QC164	164	N	353.1	67.9	355.1	-4.9	58	6	3
15QC162	162	N	356.1	40.2	356.6	-3.4	30.3	6	5.2
15QC160	160	N	0.6	68.5	0.4	0.4	58.5	6	4
15QC158	158	N	4.2	60.7	3.2	3.2	50.8	5	2.3
15QC157	157	N	28.5	70.7	19.3	19.3	61.5	5	3.8
15QC155	155	N	355.6	68.9	356.8	-3.2	58.9	5	2.8
15QC153	153	N	32.2	62.8	24.5	24.5	54	5	3.9
15QC151	151	N	359.4	67.5	359.6	-0.4	57.5	6	8.2
15QC149	149	N	1.3	69.3	0.9	0.9	59.3	6	3.3
15QC139	139	R	170.2	-65	172.7	172.7	-55.1	6	2.4
15QC135	135	R	157.2	-48.4	160.7	160.7	-39.1	6	15.3
15QC131	131	r	274.1	-51	261.9	261.9	-50.7	5	27.8
15QC129	129	n	178.6	-70.8	179.1	179.1	-60.8	5	34.4
15QC125	125	R	189.7	-46.1	188.3	188.3	-36.2	6	4.8
15QC123	123	N	15.6	51.6	12.9	12.9	41.9	6	4.9
15QC117	117	N	349.4	43.7	350.8	-9.2	33.8	8	8
15QC104	104	N	346.9	42.3	348.5	-11.5	32.5	9	2.8
15QC96	96	N	13.7	49.7	11.5	11.5	39.9	7	4.9
15QC84	84	N	337.3	61.3	342.4	-17.6	51.9	9	3.3
15QC82	82	N	29.1	51.9	24.2	24.2	42.9	7	4.3
15QC80	80	N	16.5	52.4	13.6	13.6	42.7	7	5.6
15QC79	79	N	348.8	70.6	352.4	-7.6	60.8	6	
15QC77	77	n	6.8	21	6.4	6.4	11	7	4.8

Sample	Stratigraphic Height (m)	Polarity	Geologic		Stratigraphic			# of data points used	MAD
			declination	inclination	declination	adjusted declination	inclination		
15QC70	70	N	22	59.3	17.3	17.3	49.9	6	8.9
15QC69	69	N	333	58.1	338.6	-21.4	49	7	2
15QC67	67	N	338	50.1	341.5	-18.5	40.7	7	2.8
15QC65	65	N	2.9	36.7	2.6	2.6	26.7	7	7.5
15QC63	63	N	20.4	58.4	16	16	49	5	6.5
15QC61	61	N	347.5	65.2	350.8	-9.2	55.3	8	3.3
15QC59	59	N	329.3	73.4	340.3	-19.7	64.3	6	2.1
15QC57	57	N	358	54.8	358.3	-1.7	44.8	8	4.4
15QC56	56	N	343.1	54.1	346.2	-13.8	44.5	7	2.8
15QC53	53	N	352.9	43.4	353.8	-6.2	33.5	7	2.4
15QC50	50	N	345.9	36.3	347.3	-12.7	26.5	6	8.1
15QC48	48	N	8.4	49.3	7.1	7.1	39.4	9	3.8
15QC46	46	n	289.7	77.8	320.3	-39.7	71.8	8	8.4
15QC43	43	N	355.2	48.8	355.9	-4.1	38.8	8	2.7
15QC41	41	N	335.6	50	339.5	-20.5	40.7	7	3.6
15QC39	39	n	61.1	57.3	49.5	49.5	51.6	8	7.2
15QC37	37	N	353.7	43.7	357.1	-2.9	34.6	8	3.5
15QC32	32	N	15.9	42.4	16.5	16.5	32.5	8	4.1
15QC27	27	N	5.9	48.1	8	8	38.3	6	4.5
15QC25	25	N	4	37.1	5.7	5.7	27.4	8	3
15QC23	23	N	338.5	53.2	345.6	-14.4	45.3	6	6.1
15QC19	19	N	307.6	79.2	341.6	-18.4	73.3	5	6.5
15QC18	18	N	350.5	51	355.4	-4.6	42	8	7.9
15QC17	17	N	13.7	58.1	14.9	14.9	48.1	7	8.9
15QC9	9	N	325.6	60.9	337.4	-22.6	54.3	9	1.8
15QC8	8	N	326.2	50.5	334.5	-25.5	44	7	5.1
15QC7	7	N	2.9	66	7.5	7.5	56.3	7	5.4
15QC6	6	N	337	61.7	346.8	-13.2	53.9	8	5.6
15QC5	5	N	337.3	61.4	346.9	-13.1	53.6	6	6.3

Table 4: Stable Isotope Data

Strat. Height (m)	Age (Ma)	δ18O (‰)	Strat. Height (m)	Age (Ma)	δ18O (‰)	Strat. Height (m)	Age (Ma)	δ18O (‰)	Strat. Height (m)	Age (Ma)	δ18O (‰)
477	1.78		359	2.41	1.36	309	2.65	0.62	226	3.02	-0.36
474	1.79	-0.79	357	2.42	-2.97	308	2.65	4.7	225	3.03	-1.25
473	1.80	3.73	355	2.43	-11.63	307	2.66	4.57	224	3.03	-0.95
472	1.80	-0.12	354	2.43	-2.7	306	2.66	2.63	224	3.03	-2.23
462	1.84	6.55	341	2.50	-2.18	305	2.66	-0.64	223	3.03	-0.05
459	1.86	2.04	340	2.50	-2.49	304	2.67	-5.54	222	3.04	1.52
459	1.86	2.04	339	2.51	0.05	301	2.68	-0.85	222	3.04	-0.89
458	1.86	-8.4	338	2.51	-3.63	300	2.69	1.6	221	3.04	3.22
458	1.86	-7.78	337	2.51	-1.48	300	2.69	1.59	220	3.04	-0.8
449	1.90	1.46	336	2.52	0.68	299	2.69	-0.46	219	3.04	-3.92
449	1.90	1.76	335	2.52	-2.83	298	2.70	-1.57	218	3.04	-2.32
448	1.91	-2.9	334	2.53	-2.22	297	2.70	-0.91	218	3.04	-2.21
447	1.91	3.09	333	2.53	0.07	296	2.71	-1.64	217	3.04	-4.09
447	1.91	3.94	331	2.54	1.69	241	2.95	-2.2	216	3.05	-0.53
447	1.91	4	330	2.55	-0.24	240	2.96	0.4	216	3.05	-2.22
443	1.93	6.7	329	2.55	-3.59	239	2.96	-1.25	215	3.05	0.7
441	1.94	0.31	329	2.55	-3.03	238	2.97	-1.3	214	3.05	3.51
441	1.94	0.58	328	2.56	-1.39	237	2.97	-3.66	214	3.05	0.34
437	1.97	6.1	327	2.56	-2.99	236	2.98	1.09	213	3.05	4.45
436	1.99	0.39	326	2.57	1.35	235	2.98	-4.94	213	3.05	0.74
435	2.00	0	321	2.59	6.08	234	2.99	-3.28	212	3.05	-0.89
435	2.00	-0.32	318	2.61	-3.63	233	2.99	-3.13	211	3.05	0.01
434	2.02	-1.65	317	2.61	-1.85	232	3.00	-1.23	211	3.05	0.22
420	2.14	0.37	316	2.61	-4.94	231	3.00	1.22	210	3.06	-1.19
414.5	2.14	1.63	315	2.62	-5.03	230	3.00	-1.43	210	3.06	-1.94
404	2.19	6.66	313	2.63	0.51	229	3.01	-2.6	209	3.06	-3.25
401	2.20	0.4	312	2.63	-6.47	228	3.01	-2.17	208	3.06	-2.58
361	2.40	-2.82	311	2.64	3.33	227	3.02	3.21	208	3.06	-2.12
361	2.40	-2.51	310	2.64	4.97	227	3.02	2.94	207	3.06	-5.37

Strat. Height (m)	Age (Ma)	δ18O (‰)	Strat. Height (m)	Age (Ma)	δ18O (‰)	Strat Height (m)	Age (Ma)	δ18O (‰)	Strat Height (m)	Age (Ma)	δ18O (‰)
206	3.06	-3.07	156	3.17	-0.73	78	3.43	0.83	16	3.56	0.02
206	3.06	2.43	154	3.18	-0.66	76	3.43	0.7	9	3.58	-3.34
206	3.06	-2.25	152	3.18	-2.76	71	3.44	2.63	9	3.58	-3.49
206	3.06	-3.07	150	3.19	-0.49	71	3.44	1.78	8	3.58	-0.63
204	3.07	-0.08	150	3.19	-0.7	69	3.45	-2.54	6	3.58	-2.04
204	3.07	1.89	148	3.20	0.68	67	3.45	-2.19	4	3.59	3.66
202	3.07	3.64	144	3.21	-0.52	65	3.46	-1.07	4	3.59	2.61
199	3.08	1.1	141	3.22	-4.66	63	3.46	-1.9	2	3.59	2.6
197	3.08	5.62	141	3.22	-5.59	61	3.46	0.11	0	3.60	-2.19
197	3.08	5.08	139	3.24	-2.81	59	3.47	-2.17			
195	3.08	0.19	137	3.25	2.1	59	3.47	-2.78			
193	3.09	-0.55	134	3.27	-1.81	55	3.48	-1.07			
191	3.09	-1.81	134	3.27	-1.33	55	3.48	-0.83			
189	3.09	3.55	132	3.28	-0.75	53	3.48	0.75			
187	3.10	3.92	131	3.28	-0.8	50	3.49	-2.7			
186	3.10	5.45	129	3.29	-2.26	48	3.49	-1.96			
186	3.10	4.68	127	3.31	-0.81	46	3.50	-0.93			
184	3.10	-0.71	125	3.32	-1.85	46	3.50	-1.35			
182	3.11	-3.76	123	3.33	-1.12	43	3.50	-1.43			
180	3.11	-1.36	117	3.34	-0.46	41	3.51	3.34			
177	3.11	-3.16	109	3.36	0.92	41	3.51	3.07			
176	3.12	-1.19	104	3.37	-1.18	39	3.51	-5.43			
174	3.12	-0.83	90	3.40	-0.91	37	3.52	1.73			
170	3.13	0.74	90	3.40	-1.19	32	3.53	-1.68			
168	3.14	-2.18	86	3.41	4.56	30	3.53	-2.03			
166	3.14	1.52	86	3.41	3.19	28	3.54	5.39			
166	3.14	1.73	84	3.41	0.03	27	3.54	1.29			
164	3.15	-0.85	82	3.42	-0.44	23	3.55	3.59			
162	3.16	-0.56	80	3.42	-3.94	23	3.55	3.83			
160	3.16	-0.9	78	3.43	0.55	21	3.55	0.88			
158	3.17	-1.51	78	3.43	0.64	19	3.55	1.73			

APPENDIX C

Miocene: Deep Lake Facies

Miocene age deep lake facies, dominated by thinly-bedded siltstones, mudstones and limestones, were identified in central Qaidam Basin (Wang et al., 2012). The outer margins of the basin showed higher energy deposition, including lake shore, fan and delta facies (Wang et al., 2012). This indicates that, during the warm and wet climatic conditions of the Early – Middle Miocene, the entire northwestern side of the Qaidam Basin contained one massive lake, or a system of large lakes, with an active shoreline near the surrounding mountain along the boundaries of the basin (Kezao and Bowler, 1986; Wang et al., 2012).

Pliocene: Shifting towards aridification

Between the Late Miocene and the Pliocene, the lake system slowly dwindled and shifted southeast (Kezao and Bowler, 1986). The presence of lacustrine facies, dominated by mudstone and sandstone, in the lower strata of the Shizigou Formation indicate that deep lakes were still present in northeast Qaidam Basin through the early Pliocene, though they were likely isolated (Heermance et al., 2013, Wang et al., 2012). Subsequent appearance of fluvial and evaporitic facies indicate a general lowering of lake levels throughout the Pliocene as regional aridity increased. By the late Pliocene, the northern Qaidam Basin was host to multiple small playas (Heermance et al, 2013; Kezao and Bowler, 1986). The presence and repetition of interlayered strata consisting of calcareous mudstones (lacustrine deposition) and evaporite formation (playa deposition) also shows frequent fluctuations in lake-levels during this long-term trend towards aridification

(Kezao and Bowler, 1986; Li et al., 2013). This surface water fluctuation is an environmental response to regional climatic oscillations, which indicates recurring short-term (10^4-10^6 years) intervals of warm/wet and cold/dry conditions, likely driven by orbital forcing mechanisms (Heermance et al. 2013; Riegel, 2015; Zachos et al. 2001).

Pleistocene/Holocene: Transition to Complete Aridification

After 2.6 Ma, the strata from a playa in northeastern Qaidam Basin is dominated by evaporite rich mudstone with increasing evaporite concentrations upsection (Heermance et al., 2013). Large deposits of halite and gypsum crystals in the Qigequan Formations indicate that the lake completely dried up during the Holocene, effectively ending the development of the lake cycles (Heermance et al., 2013; Kezao and Bowler, 1986; Wang et al., 2012).

APPENDIX D

Eccentricity (100 kyr and 400 kyr)

The shape of Earth's orbital path around the sun is not constant. It shifts between a more circular (low eccentricity) path and a more elliptical (high eccentricity) path. When orbital eccentricity is high, Earth can be closer to, or further away from the Sun at different locations along the orbital path (Ruddiman, 2008). This can alter the amount of solar insulation received by the earth throughout the year (Berger, 2006). Eccentricity orbital forcing produces 95 kyr and 131 kyr cycles, which average to a dominant 100 kyr cycle frequency. Additionally, 413 kyr cycles can appear as the 100 kyr peak values fluctuate (Riebeek, 2006; Ruddiman, 2008).

Obliquity (41 kyr)

Earth's axis is tilted away from the ecliptic, which angles the Northern Hemisphere or the Summer Hemisphere towards the sun during different times of the year. It is currently tilted at 23.5°, but it can vary between ~22° and ~24° (Ruddiman, 2008). While obliquity does not affect the amount of solar insulation received by Earth, it does affect its distribution. Higher obliquity can distribute solar insulation to higher and lower latitudes (Riebeek, 2006). Obliquity orbital forcing produces 41 kyr cycles.

Precession (23 kyr)

The tilt in Earth's axis produces seasons, and as earth rotates around the sun the orbital location of the Norther Hemisphere and Southern Hemisphere summers are shifted. This gradual change is called procession of the equinox (Riebeek, 2006).

Precession orbital forcing produces 19 kyr, 21 kyr and 24 kyr climate cycles, which average to a 23 kyr dominant cycle frequency (Ruddiman, 2008).

The climatic effects of precession orbital forcing can be amplified or dampened by eccentricity. With very low eccentricity, shifting the orbital location of the equinox has little affect Earth's net insulation. However, with high eccentricity, procession can cause (1) cold winters coupled with hot summers, or (2) warm winters coupled with cool summers (Ruddiman 2008). This eccentricity modulated precession is classed axial precession forcing, which can also produce 26 kyr cycles, with larger scale 100 kyr and 400 kyr cycles (Riebeek, 2006).

APPENDIX E

MAGNETOSTRATIGRAPHIC ANALYSIS OF SEDIMENTARY ROCKS

Paleomagnetism and Magnetic Stratigraphy

Although the Earth's magnetic field is incredibly complicated, it is reasonable to assume the dipole hypothesis for this study (Buttler, 1992). The orientation of the geomagnetic field at any given time is recorded by paramagnetic, ferromagnetic and diamagnetic ions within rocks, recording either reversed polarity (declination south and inclination up), or normal polarity (declination north and inclination down), as is observed today (Opdyke and Channell, 1996). Analysis of the paleomagnetic signature of rock samples throughout a stratigraphic section will yield a magnetic stratigraphy, which can be correlated to geomagnetic polarity timescale (GPTS) to identify the age of the rock sample (Opdyke and Channell, 1996).

Remanent Magnetization

A rock can acquire a magnetic signature through many different processes. Primary magnetization of a sedimentary rock is acquired through detrital remanent magnetization (DRM), which is acquired during the deposition of the sediment and locked in place during lithification (Tarling and Turner, 1999). Post-depositional remanent magnetization (pDRM) can alter the magnetic alignment of sediment prior to lithification if there is sufficient alteration due to bioturbation or other external factors (Opdyke and Channell, 1996). There are other post-depositional processes that can affect the paleomagnetic signature of sedimentary rocks including: chemical remanent magnetization (CRM), which involves the magnetization of ferromagnetic crystals formed within an existing rock; isothermal remanent magnetization (IRM), which occurs

when the magnetization of a rock is reset because the magnetic components are exposed either to intense heat above their Curie Temperature, or to a particularly strong magnetic field; and viscous remanent magnetization (VRM), which occurs when weaker magnetic components are reset due to prolonged exposure to an external field (Butler, 1992; Opdyke and Channell, 1996). Thermoremanent magnetization (TRM) is another process that can alter the primary magnetization of a sample, but this is more common in igneous than in sedimentary rocks (Opdyke and Channell, 1996). Each of the above listed components of remanent magnetization contribute to the in situ natural remanent magnetization (NRM) of a rock (Butler 1992).

Paleomagnetism in Qaidam Basin

Assuming application of the dipole hypothesis is reasonable, the expected inclination for samples within the Qaidam Basin (37°42'50" N, 92°22'45" E) can be calculated using:

$$\mathbf{Tan\ (I) = 2\ Tan\ (\lambda)}$$

where I = inclination, and λ = latitude (Opdyke and Channell, 1996). The resulting inclination is 56.9°. Therefore, expected values for the samples collected in the in the QC section of the Qaidam Basin are declination = 0° and inclination = 56.9° for normal polarity, and declination = 180° and inclination = -56.9° for reverse polarity. Inclination shallowing, caused by compaction of sediments, is a common occurrence, and it has been recorded in previous paleomagnetic studies within the Qaidam Basin (Fang et al., 2007; Heermance et al., 2013; Zhang et al., 2012).

APPENDIX F

DETAILED METHODS

Field Work: Sample and Data Collection

The entire stratigraphic thickness that has been exposed in the QC section, from the core of the anticline to the layer of active deposition, spans ~740 m and consists of a lower and an upper segment that overlap between 201 m and 226 m in stratigraphic height (Figure 1). From 0 m - 540 m, the stratigraphy was measured using a 1.5 m Jacob Staff, an Abney level and a Brunton compass; and described using a Munsell color chart and a USGS grain size chart. The remaining ~200 m were inferred as similar material to that observed at 500 m - 540 m, capped by the layer of active deposition at ~740 m. From 0 m - 477 m, the strata were sampled for paleomagnetic and stable isotopic analysis.

Field work in the QC section was completed on three separate trips. In April of 2015, the upper segment (201 m – 540 m in stratigraphic height) was measured and described, and it was sampled in 24 locations for reconnaissance paleomagnetic analysis. In the summer of 2015, the lower segment (0 m – 226 m in stratigraphic height) was measured and described, and 330 samples were collected from 173 locations throughout the lower and upper segments of the QC section. In total, 327 core samples were collected with a rock coring drill, and 3 block samples were collected using a rock hammer. High resolution sampling (i.e. 1 sample every 1-2 stratigraphic meters) was taken whenever continuous, good quality outcrops were available; however, there are areas throughout the QC section where no outcrops are accessible, yielding an average sample spacing of ~2.5 m. GPS coordinates were taken for all 197 sampling location. A final trip was made in December of 2016 to physically correlate the upper and lower segments, and to address uncertainties in the stratigraphic record.

The Composite Stratigraphic Column

The upper and lower segments of the QC section were measured and described by different people on separate field visits. The two segments were correlated by 1) tracing resistant beds remotely using Google Earth, 2) connecting paleomagnetic reversal sights within the overlapping strata, 3) connecting lithofacies sequences within the overlapping strata, and 4) physically tracing resistant beds in the field. In addition, photographs associated with certain rock descriptions from each trip were compared and categorized in order to maintain a consistent classification of major lithofacies.

The Magnetostratigraphic Record

Paleomagnetic Analysis

290 core and block samples were cut in the CSU Northridge Rock Cutting Laboratory into 1.5 cm diameter rounds, 1-2 inches in thickness. 235 samples were processed for paleomagnetic signatures using the 2G Cryogenic Magnetometer at Occidental College Paleomagnetic Laboratory. Samples with labels beginning with "QC" were initially processed once for Natural Remnant Magnetization (NRM), and then for Alternating Field (AF) demagnetization at 25, 50, 100 and 200 oersteds (oe) to begin to remove viscous magnetic components (Opdyke and Channell, 1996). These samples were then heated in the laboratory oven and processed for Thermal Demagnetization (TT) at the following temperatures: 150°, 200°, 250°, 300°, 350°, 400°, 450°, 500°, 530° and 560° C. The approach was refined for subsequent samples with labels beginning with 15QC, which were initially processed three times for NRM. Between each NRM step, the samples were submerged in liquid nitrogen, which removes viscous magnetic

components (Borradaile et al, 2004). These samples were also processed for AF at 25, 50, 100 and 200 oe to remove additional viscous components. 15QC samples were then heated and processed for TT a the following temperatures: 200°, 300°, 400°, 450°, 500°, 530°. All samples began to show high processing errors due to low magnetization by ~500° C, and were sufficiently demagnetized by ~530° C.

The data collected with the cryogenic magnetometer were analyzed using the PaleoMag 3.1d35 program, which uses paleomagnetic data to identify the primary magnetic polarity of each sample. Visual analyses of the data were completed using tilt-corrected orthographic, equal area and J/J0 demagnetization plots to isolate the non-viscous magnetic components, which are likely indicative of the primary magnetic signature. Statistical analyses of these non-viscous magnetic components were done using a least squares fit line (excluding the origin), to calculate the geographic declination and inclination, the stratigraphic declination and inclination, and the error (maximum angle of deviation [MAD]) for each sample.

The results of the statistical analysis identify the magnetic polarity of each sample as either normal (north and down) or reversed (south and up), and categorized each sample into one of three groups: robust, tentative, and uninterpretable signatures. Expected values for the samples collected in the in the QC section of the Qaidam Basin are declination = 0° and inclination = 56.9° for normal polarity, and declination = 180° and inclination = -56.9° for reverse polarity (Opdyke and Channell, 1996). Each sample is categorized based on both visual and statistical analysis. Samples with robust signatures show two magnetic components (primary and viscous), and they generally have stratigraphic declination and inclination values that are within 10° of expected

values and an MAD value $\leq$ 10. Samples with tentative signatures generally show two magnetic components, and they have stratigraphic declination and inclination values that are within 20° of expected values and an MAD value $\leq$ 20. Samples that do not meet the above listed criteria are identified as uninterpretable, and are not used in the process of assembling the magnetostratigraphic record. The inclination and declination for samples with interpretable signatures (both robust and tentative) were graphed and used to produce the QC magnetic stratigraphy.

Magnetic Stratigraphy: Assumption of Young Strata

Studies have been conducted in the Qaidam Basin that constrain the majority of basin deposition to the Late Cenozoic (Kezao and Bowler, 1986; Wang et al., 2012). The Plio-Quaternary age range for the QC section that has been identified in this study (3.6 Ma – 1.8 Ma) is consistent with studies that have focused on playa-lacustrine deposition in other areas within the Qaidam Basin (Heermance et al., 2013; Riegel, 2015; Wang et al., 2012). Additionally, the proximity of the measured strata (0 m – 540 m) to the layer of active deposition (~740 m) indicates that the QC section must be relatively young in age.

Magnetic Stratigraphy: Correlation to Global Events

The transition in the stratigraphic column from Unit 3 to Unit 4 at 300 m, identified by the onset of limestone deposition and increasing evaporitic content, indicates a significant shift in the sedimentological record. A 3.6 Ma – 1.8 Ma age range correlates this major shift in lithology to the Plio-Quaternary Boundary (~2.6 Ma). In addition, within Unit 2 (120 m – 185 m), thick M1 and M2 deposits occur in the same stratigraphic location as relatively low and stable $\delta^{18}O$ values, both of which indicate higher lake

levels during a warm and wet climate. Applying the 3.6 Ma – 1.8 Ma age range to the stratigraphic heights for Unit 2 places this warm and wet period between 3.33 and 3.1 Ma, which correlates well to the globally recognized Mid-Piacenzian warm period (Salzmann et al, 2011).

Magnetic Stratigraphy: Calculations and Statistical Analysis

Supplementary evidence to support this Plio-Quaternary age range is shown through the calculation of reasonable sedimentation rates when comparing the stratigraphic height of each magnetic reversal to the known age of that reversal event (see section *4.4.1 Sedimentation Rates* for more information). Additionally, the magnetic stratigraphy data was analyzed using the Qupydon program, which statistically evaluates possible GPTS correlations. The Qupydon results identified 3.6 Ma – 1.8 Ma as one of the most likely age range options.